Geologica Acta, Vol.9, Nos 3-4, September-December 2011, 273-287
DOI: 10.1344/105.000001715
Available online at www.geologica-acta.com

geologica acta

Pre-arc basement complex and overlying early island arc strata, Southwestern Puerto Rico: overview, geologic evolution, and revised data bases

E.G. LIDIAK [1] **W.T. JOLLY** [2 ‖ †] **A.P. DICKIN** [3]

[1] **Department of Geology and Planetary Science, University of Pittsburgh**
Pittsburgh, PA., USA 15260 E-mail: egl@pitt.edu

[2] **Department of Earth Sciences, Brock University**
St. Catharines, Ontario, Canada L2S 3A1

[3] **Department of Geography and Geology, McMaster University**
Hamilton, ON CANADA L8S 4M1 E-mail: dickin@mcmaster.ca

† Deceased

ABSTRACT

The pre-arc basement complex in southwestern Puerto Rico consists of rocks exposed in the Bermeja complex. The oldest rocks are highly serpentinized peridotites that occur in three belts (Monte del Estado, Río Guanajibo, and Sierra Bermeja). These serpentinites were emplaced into a sequence of Jurassic to mid-Cretaceous pelagic chert (Mariquita chert) that contains abundant rafts and blocks of N-MORB-type amphibolites (Las Palmas amphibolite) and tholeiite and associated trondhjemite fractionates (Lower Cajul MORB) also of N-MORB affinity. The rocks are apparently overlain by a younger sequence of pre-arc plateau basaltic and andesitic lava flows (Upper Cajul Formation) that occur in two distinct geographic sequences, one having E-MORB and the other OIB geochemical characteristics. Overlying these pre-arc rocks in western Puerto Rico are northwest-trending Late Cretaceous to Eocene (85 to 45Ma) island arc strata that chronologically overlap later volcanic phases in central Puerto Rico. These western Puerto Rico arc rocks have elevated incompatible element concentrations together with conspicuously shallow negative Nb-anomalies, slightly positive Zr-Hf anomalies, and exceedingly high OIB-like Nb/Zr, all indicative of enriched source compositions. Trace element patterns are reproduced by multiple component mixing models involving highly depleted spinel peridotite (RMM15 to 20) overprinted by small OIB-type (up to ~2%) and pelagic sediment components. Trace element abundances are too high to qualify Atlantic Cretaceous pelagic sediment as a potential contaminant, but mantle-melting models (f=0.25) are consistent with the incorporation of variable proportions of Caribbean Cretaceous pelagic sediment through north-dipping subduction of the Caribbean basin. Anomalous two-pyroxene-bearing andesites with extraordinarily high SiO_2/MgO compared with normal mantle basaltic compositions, also indicate the incorporation of Jurassic to Early Cretaceous pelagic chert from the Caribbean. The high degree of source enrichment in western Puerto Rico is inconsistent with regional within-plate plume tectonics. Instead, it is inferred that the younger north-dipping western Puerto Rico arc (dating from ~85Ma) sampled an upper mantle enrichment zone generated in the back-arc region of the older (125 to ~85Ma) south-dipping arc system in central Puerto Rico.

KEYWORDS | **Caribbean. Island Arc. Ophiolite Complex. Pelagic Sediment. Subduction.**

INTRODUCTION

The Greater Antilles Island Arc platform, which represents the only major Mesozoic destructive plate margin associated with the North Atlantic Ocean, forms the long-lived and fragmented northern boundary of the Caribbean Plate. Preserved within the platform in Puerto Rico are both 1) pre-arc thoeliitic basalt and associated amphibolite of oceanic crustal origin (Fig. 1, 2) a pair of independent, partly simultaneous but geochemically distinct island arc systems, one with depleted N-MORB affinities (central Puerto Rico, northeast Puerto Rico) (Jolly et al., 2008a) and another with highly enriched, OIB-like compositions (western Puerto Rico) (Jolly et al., 2007). Consequently, an understanding of the pre-arc geochemical characteristics prior to the development of the island arc sequences in the Antilles is important in helping to resolve the tectonic relations both within and among the islands of Cuba (Iturralde-Vinent, 1998; García-Casco et al., 2006; Proenza et al., 2006; Marchesi et al., 2007), Hispaniola (Lewis et al., 2002), Jamaica (Draper, 1986; Mitchell, 2006), and Puerto Rico (Jolly et al., 1998b, 2007; Schellekens, 1998), and in interpreting interactions between the adjacent North American and Caribbean Plates. The regional role of an incompatible element enriched OIB-type component in the Antilles mantle wedge, for example, remains an important question. Equally significant are the geochemical links between arc lavas and subducted Atlantic and Caribbean Mesozoic pelagic sediments. The data presented in this study addresses the geochemical characteristics of the older rocks of the western Puerto Rican segment of the Greater Antilles island arc.

The specific objectives of this investigation are to provide an updated overview of the older rocks that compose the pre-arc complex of southwestern Puerto Rico, to evaluate the geologic and geochemical evolution of the immediately overlying island arc sequence, to make minor revisions in the stratigraphic nomenclature for enhanced clarity, to correct errors in several published databases, and to present previously unpublished datasets for these older rocks.

GEOLOGICAL SETTING

The island of Puerto Rico is located south of the broad, structurally diffuse Puerto Rico Trench Megathrust (Fig. 1A), and north of the west-trending Los Muertos Trench Thrust, which respectively represent the north and south boundaries of the Puerto Rico-Virgin Islands block. The Greater Antillean islands of Hispaniola, Jamaica, and Cuba lie west of Puerto Rico. To the east are the Virgin Islands and the modern Lesser Antilles arc. The Puerto Rico block or microplate (Jansma et al., 2000) bridges the transition between these two segments.

Volcanic strata in eastern and central Puerto Rico are distributed within five west-trending volcanic belts, representing principal volcanic axes during discrete eruptive phases (volcanic phases I through V) (Jolly et al., 1998b; Schellekens, 1998) and ranging in age from Aptian to Late Eocene (120 to 45my). Predominant westerly trends in central Puerto Rico are truncated by the northwest-trending Greater Southern Puerto Rico Fault Zone (Glover, 1971) and sub-parallel volcanic belts in western Puerto Rico. The Sierra Bermeja Complex of western Puerto Rico incorporates rock types associated with ocean basins, including partly serpentinized spinel peridotite (Mattson, 1979; Jolly et al., 1998b) that occupies three main belts (Monte del Estado ((Electronic Appendix Table I, available in www.geologica-acta.com)), Río Guanajibo, and Sierra Bermeja; Fig. 1B). The Mesozoic oceanic basement complex is succeeded by western Puerto Rico arc strata dating from Santonian time (Jolly et al., 2007), the distribution of which is shown in Figure 1C. The serpentinites were periodically emplaced along with arc volcanism from Santonian to Late Eocene time (Krushensky and Monroe, 1978; Martinez-Colon, 2003).

FIGURE 1 | **Map of the Caribbean region showing principal structural elements of the tectonic boundary between the North American - Carribean Plates (lines represent fault zones, teeth represent polarity of subduction zones. The vector, indicating motion of the Atlantic Basin with respect to a stable Caribbean, is from Jansma et al. (2000). Locations of DSDP drilling sites within the Caribbean Cretaceous Basalt Plateau (CCBP) are indicated. Contours in the Caribbean Basin represent thickness (km) of oceanic crust (seismic velocity < 7.4km/sec; Mauffret and Leroy, 1997). "X" represents the Sierra de Bahoruco region, from which representative Caribbean Late Cretaceous pelagic sediment (CKPS, Río Arriba Fm. (Llinas, 1972) was collected. Additional features identified as follows; AF: Anegada Fault; AI: Aves Island; CLIP: Caribbean large igneous province of Hauff et al. (2000); CT: Cayman Trough spreading center; GP: Gonive Microplate; HS: Hispaniola microplate; LMTT: Los Muertos Trench Thrust; MP: Mona Passage; PR: Puerto Rico; PRTMT: Puerto Rico Trench Megathrust; PR-VI: Puerto Rico - Virgin Islands Microplate; SITF: Swan Island Transform Fault; WF: Walton Fault. B) Map of tectonic elements in western Puerto Rico (WPR), including serpentinized peridotite (purple hachure pattern), Jurassic pelagic chert (yellow stipple), MORB basalt (black), back-arc strata (parallel), volcanic arc strata (green shaded); other symbols include; A: amphibolite; BQN: Boquerón Fm.; C: chert; PL: Parguera Ls (includes lesser IAB volcanic strata and plutonic rocks); E: Eocene Jicara Fm. (shale); LJS: Lajas Fm.; QT and Q: Quaternary alluvium; RL: Río Loco Lava (green parallel dots); S: serpentinite; V: volcanic rocks. Tectonic block names adopted from synformal terminology of Mattson (1960). C) Sierra Bermeja region, southwest Puerto Rico illustrating exposures of serpentinized spinel peridotite mélange containing numerous blocks of amphibolite (SP), Mariquita Chert (MQT), Las Palmas amphibolite mélange (A), and altered Cajul basalts (LCAJ, UCAJN, UCAJS-see text). Adapted and modified from Volckmann (1984a, b, c).**

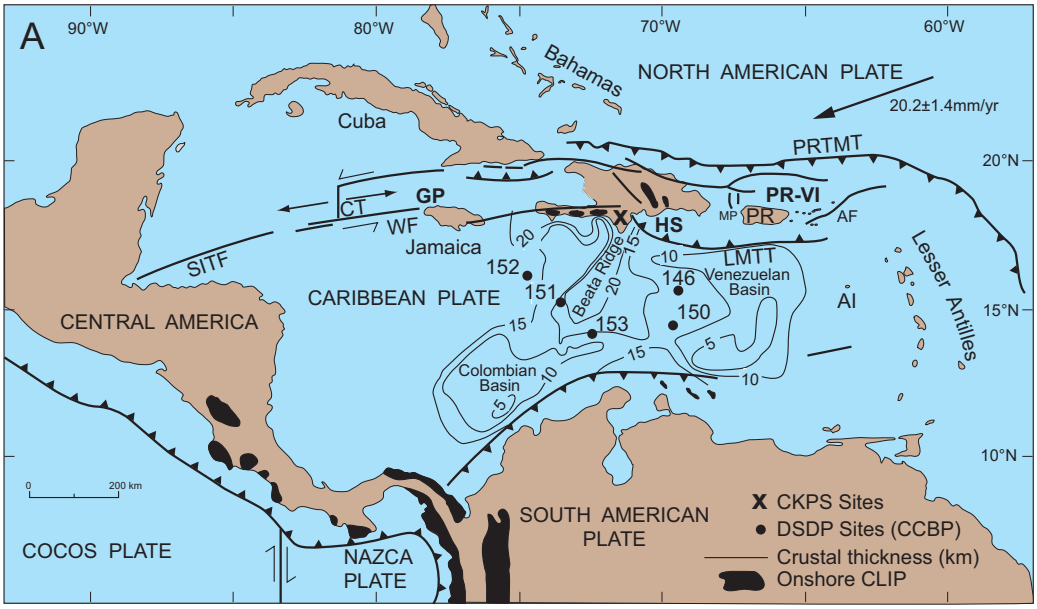
A
90°W
80°W
70°W
60°W
Bahamas
NORTH AMERICAN PLATE
20.2±1.4mm/yr
Cuba
PRTMT
20°N
GP
CT
WF
Jamaica
PR-VI
MP
PR
AF
HS
X
SITF
CENTRAL AMERICA
CARIBBEAN PLATE
Beata Ridge
LMTT
Venezuelan Basin
AI
Lesser Antilles
15°N
Colombian Basin
10°N
0
200 km
SOUTH AMERICAN PLATE
COCOS PLATE
NAZCA PLATE
X CKPS Sites
DSDP Sites (CCBP)
Crustal thickness (km)
Onshore CLIP

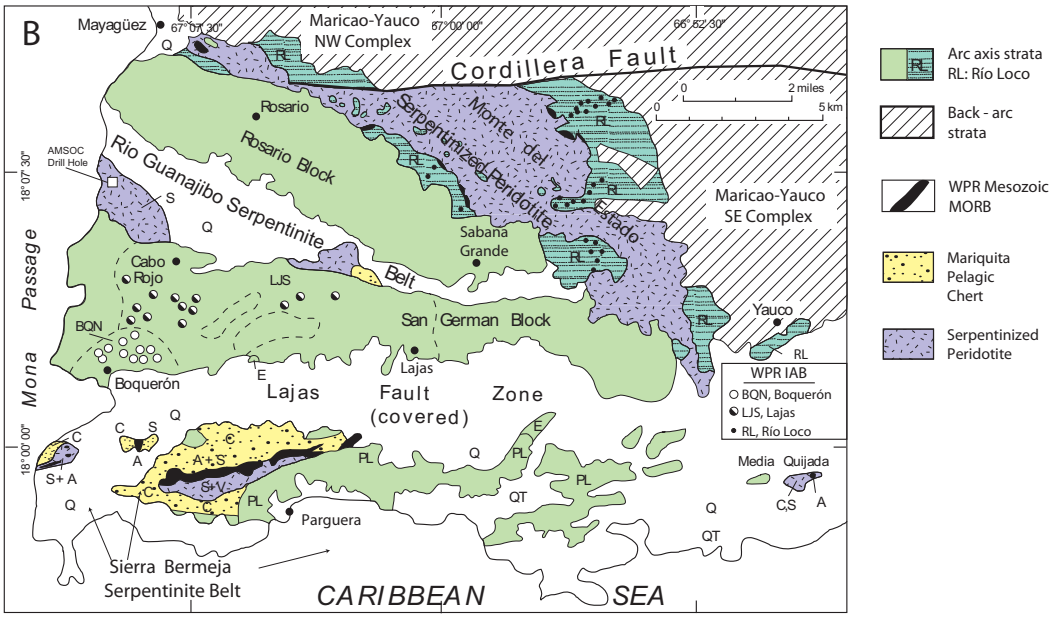
B
Mayagüez
Maricao-Yauco NW Complex
Cordillera Fault
Rosario
Rosario Block
Río Guanajibo Serpentinite
Serpentinized Peridotite
Monte del Estado
Maricao-Yauco SE Complex
AMSOC Drill Hole
Sabana Grande
Cabo Rojo
LJS
Belt
San German Block
Yauco
BQN
Boquerón
Lajas
Lajas Fault Zone (covered)
WPR IAB
BQN, Boquerón
LJS, Lajas
RL, Río Loco
Media Quijada
Parguera
Sierra Bermeja Serpentinite Belt
CARIBBEAN SEA
Mona Passage
Arc axis strata RL: Río Loco
Back - arc strata
WPR Mesozoic MORB
Mariquita Pelagic Chert
Serpentinized Peridotite

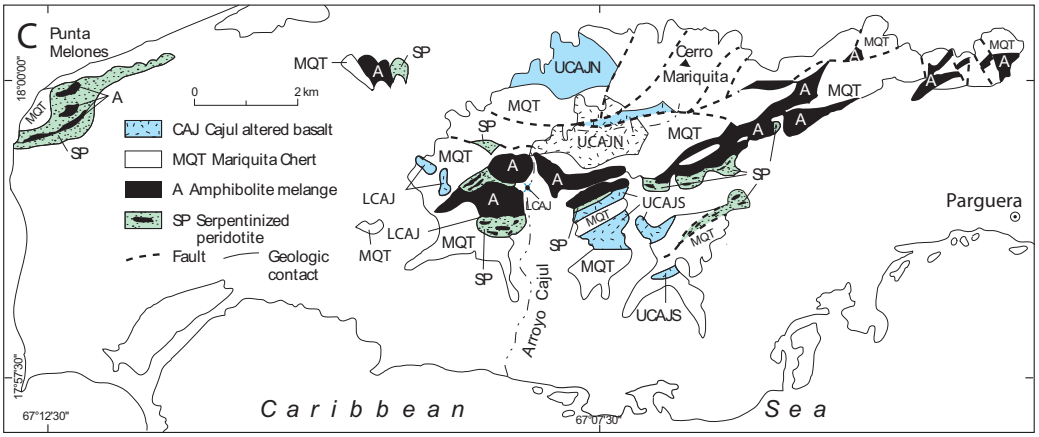
C
Punta Melones
CAJ Cajul altered basalt
MQT Mariquita Chert
A Amphibolite melange
SP Serpentinized peridotite
Fault
Geologic contact
UCAJN
Cerro Mariquita
LCAJ
UCAJS
Arroyo Cajul
Parguera
Caribbean Sea

PRE-ARC BASEMENT COMPLEX, SOUTHWEST PUERTO RICO

The pre-arc basement discussed in this report comprises the rocks exposed in the Sierra Bermeja Complex (Mattson, 1960). The oldest rocks consist of a mélange of serpentinized spinel peridotite (Schellekens et al., 1991; Jolly et al., 1998b, 2007; Schellekens, 1998). The serpentinite contains abundant blocks of N-MORB type amphibolite (Las Palmas amphibolite) (Fig. 1C, 2) and local xenolithic clasts of Jurassic tholeiitic pillow lava of N-MORB affinity (Lower Cajul MORB, LCAJ in Fig. 1C, 2). Overlying this mélange is a thick sequence of pelagic sedimentary rock (Mariquita chert) of Early Jurassic to Mid-Cretaceous age and of Pacific provenance (Montgomery et al., 1994a, b). The uppermost units in the pre-arc sequence are aphanitic basalts (Upper Cajul Formation), probably representing a local facies of the Late Cretaceous basalt plateau (Hauff et al., 2000; Kerr et al., 2002) of the Caribbean basin. The Upper Cajul basalts are the uppermost pre-arc sequence, consisting of a northern facies of plateau basalt of E-MORB affinity and a southern facies of OIB affinity (Fig. 1C, 3).

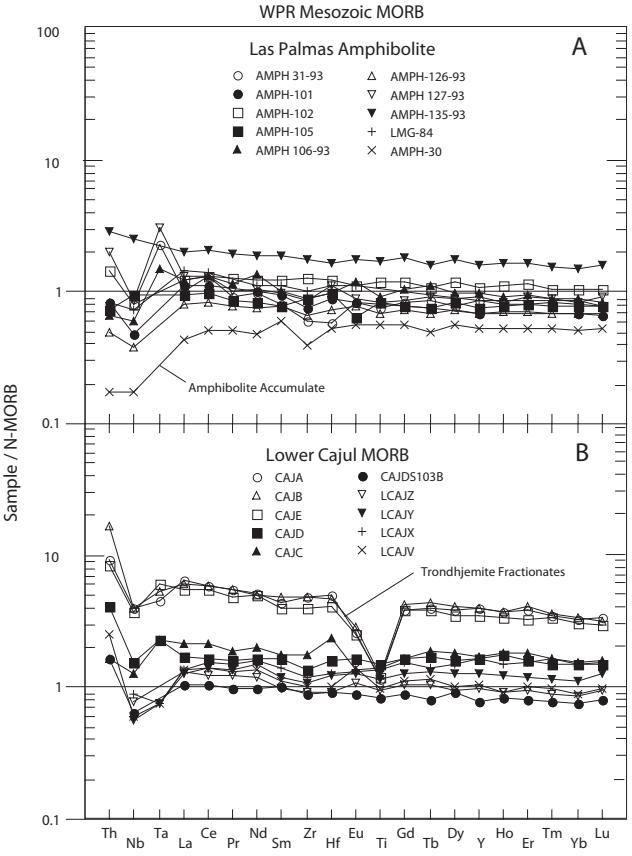

FIGURE 2 | **N-MORB-normalized incompatible element patterns. A) Las Palmas amphibolites and B) Lower Cajul MORB basalt and fractoniated trondhjemite.**

Western Puerto Rico Mesozoic MORB

Tholeiitic pillow basalt and associated trondhjemite fractionates (Lower Cajul MORB) along with massive to schistose and foliated plagioclase-hornblende amphibolite (Las Palmas Amphibolite) are prominent in the pre-arc basement in southwest Puerto Rico (Fig. 1C). The rocks occur as engulfed xenolithic blocks, reaching hundreds of meters in diameter, within marginal parts of the serpentinized peridotite (Mattson, 1960; Curet, 1986; Martínez-Colon, 2003). Amphibolite and tholeiitic pillow lavas are closely associated with the black to pale grey radiolarian Mariquita chert of Pacific provenance (Montgomery et al., 1994a) both 1) as xenolithic inclusions in serpentinite mélange, as in Sierra Bermeja and in central parts of the Monte del Estado peridotite (Llerandi-Roman, 2004), or 2) as clasts in pre-volcanic chert-amphibolite-pebble conglomerate overlying fragmental serpentinite along the north border zone of the Monte del Estado serpentinized peridotite (McIntyre, 1975). At Sierra Bermeja the basement complex is succeeded by up to 300m of pelagic chert (Mariquita Chert), ranging from mid-Jurassic (Pliensbachian, ~185Ma) to Early Cretaceous in age (Montgomery et al., 1994a). Hence, stratigraphic relations indicate the western Puerto Rico amphibolites, tholeiitic basalts and fractionates represent remnants of pre-arc Jurassic MORB (Schellekens et al., 1991; Jolly et al., 1998b) from the Mesozoic proto-Pacific (Farallon) Plate (Pindell et al., 1988; Donnelly, 1989; Pindell and Barrett, 1990; Montgomery et al., 1994a).

In conformity with the suggestion of a MORB origin, the pre-arc basalts and amphibolites have depleted normalized incompatible element patterns and compositions (Fig. 2; Electronic Appendix Tables II, IV) overlapping the N-MORB trend together with low La/Nb and La/Sm, averaging 1.7 and 1.1 respectively, similar to modern Atlantic MORB (Dosso et al., 1993), altered Cretaceous Atlantic MORB (Jahn et al., 1980) and N-MORB (0.95 and 1.1 (Sun and McDonough, 1989)). In addition, isotopic data (Appendix Table 4) reveal the rocks have uniformly MORB-like ε_{Nd}-values (average 8.3) and elevated initial $(i)^{87}Sr/^{86}Sr$ (average 0.7039), overlapping the field of altered Cretaceous Atlantic MORB (average 0.7040). The presence of normal-type Mesozoic MORB in the pre-arc basement is inferred to reflect original fertile MORB mantle type compositions in the upper mantle beneath Puerto Rico.

Upper Cajul Formation

The uppermost unit in the pre-arc basement sequence is the Upper Cajul Formation. The formation consists of two distinct geographic and geochemical facies (northern and southern) of plateau basaltic and andesitic (volatile-free basis) lava flows that are characterized by incompatible

element-enriched compositions. The contacts between the lava flows and the apparently underlying Mariquita chert are not exposed but the relative stratigraphic positions and evolved compositions suggest the Upper Cajul flows were erupted late in the pre-arc sequence. The northern facies occurs in fault blocks in the Mariquita chert, mainly along the northern flank of Sierra Bermeja (Fig. 1C), whereas the southern facies is interlayered with the Mariquita chert on the southern flank of the massif (Volckmann, 1984a). The two units probably represent local facies of the Late Cretaceous Caribbean basalt plateau that is dated at about 90Ma (Lapierre et al., 1999; Kerr and Tarney, 2005), although we do not exclude an earlier origin of these basalts.

Samples from the northern facies have normalized incompatible element patterns that approximate E-MORB patterns (Fig. 3A; Electronic Appendix Table V). Isotope data for the northern rocks are uniformly more enriched in Sr and Nd than western Puerto Rico Mesozoic MORB, containing average ε_{Nd}-values of 6.9 and elevated initial $(i)^{87}Sr/^{86}Sr$ 0.70465. In comparison, the southern facies have incompatible trace element patterns that closely coincide with OIB compositions (Fig. 3B; Electronic Appendix Table VI). Similarly, the average initial Sr and Nd ratios is slightly more evolved for the southern facies than for the northern facies, with $(i)^{87}Sr/^{86}Sr$=0.70472 and ε_{Nd}=4.7.

Caribbean Cretaceous Basalt Plateau

Presence of pelagic chert of Pacific provenance (Montgomery et al., 1994a) indicates the western Puerto Rico pre-arc crustal sequence originated within the ancient proto-Pacific (Farallon) Plate (Pindell et al., 1988; Donnelly, 1989; Pindell and Barrett, 1990; Montgomery et al., 1994a). The Caribbean Basin has subsequently undergone at least two within-plate basalt plateau-forming events (Hauff et al., 1997, 2000; Lewis et al., 2002). The oldest, Plateau I of Lewis et al. (2002), occurred concurrent with the initiation of the mid-Atlantic ridge (about 175Ma). E-MORB-type basalt produced by Plateau I were subsequently obducted onto central Hispaniola during early Albian time (Duarte Complex). A second event (Plateau II), dating between 91 to 88Ma, is correlated with the initiation of the East Pacific Rise and with widespread within-plate basalt activity comprising the Caribbean Large Igneous Province of Hauff et al. (2000) including 1) eruption and obduction of basalt along the southern Caribbean margin in Columbia and Central America, 2) mafic plutonism in Hispaniola (Siete Cabezas Complex, Lewis et al., 2002), and 3) development of the Caribbean Cretaceous Basalt Plateau in the Caribbean Basin (Donnelly, 1994). Crustal variations within the Caribbean (Fig. 1A) reveal that the Caribbean Cretaceous Basalt Plateau attains a maximum thickness of 20km along the Beata Ridge and thins laterally to less than 10km south of Puerto Rico (Mauffret and Leroy, 1997).

Seven Deep Sea Drilling Project core samples of the Caribbean Cretaceous Basalt Plateau were analyzed (Electronic Appendix Table VII). The basalts have variable trace element compositions (Fig. 4). Samples from sites 146, 150, 152, and 153 (Fig. 1A) have LREE, Th, and Nb compositions between N-MORB and E-MORB, and MREE and HREE compositions approximating E-MORB. In contrast, two basalts from site 151 have LREE, MREE, Th, and Nb essentially intermediate between E-MORB and OIB.

MESOZOIC PELAGIC SEDIMENTS, ANTILLES REGION

Atlantic Cretaceous Pelagic Sediment

Eight Atlantic Cretaceous pelagic sediment samples from the Deep Sea Drilling Project drill cores at sites 105 and 417 in the eastern North Atlantic (Electronic Appendix Fig. I) are presented in Figure 5A and Tables 8

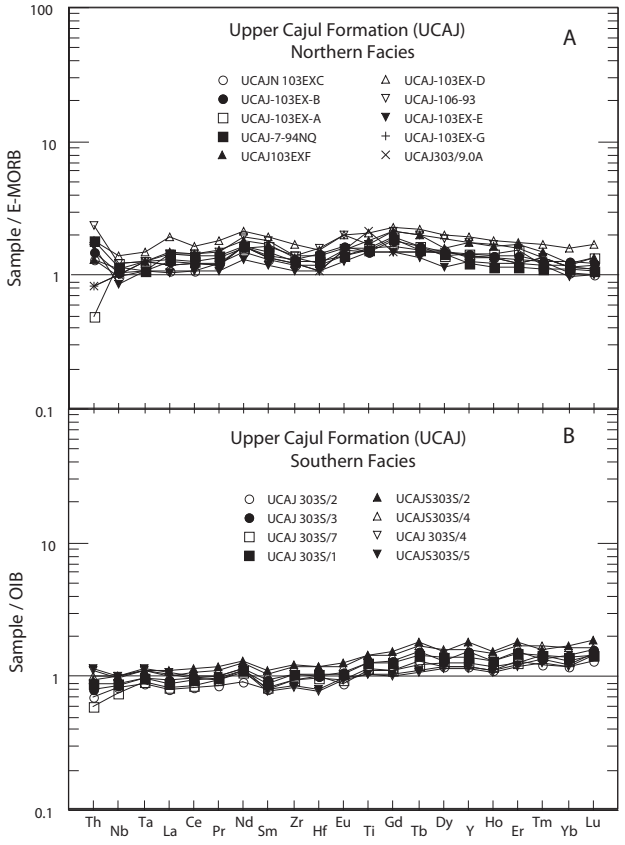

FIGURE 3 | **Normalized incompatible element patterns of Upper Cajul Formation. A) Northern facies, normalized to E-MORB and B) Southern facies, normalized to OIB.**

and 9; inferred paleontological ages are given in Jolly et al. (2008b). Total thicknesses of recovered cores averaged about 100m, of which Cretaceous sediment comprised about 65m. Proportions of analyzed samples approximate total relative abundances of Cretaceous rock types, averaging 60% claystone and 40% calcareous claystone and limestone. Earliest Atlantic strata (>150 to 110Ma) are dominated by carbonate and calcareous clay, which was supplanted by black and green claystone during Late Cretaceous time.

Pacific (Farallon) mid-Jurassic to Early Cretaceous pelagic chert

Caribbean pelagic sediment is represented in south-western Puerto Rico by radiolarian chert (Mari-quita chert) of Mid-Jurassic to Early Cretaceous age (Mattson, 1960; Llerandi-Roman, 2004), up to 300m of which occurs in the Sierra Bermeja ultramafic complex (Fig. 1B, C). Presumably correlative xenolithic chert is reported from the Monte del Estado serpentinized peridotite (Llerandi-Roman, 2004) suggesting widespread distribution within the pre-arc basement. The Mariquita chert contains from 95% to almost 100% SiO_2 (Table 8) and is extremely depleted in incompatible elements compared with Late Cretaceous pelagic sediment (Fig. 5), rendering it ineffective as a mantle contaminant, except as a dilutant. The chert has low La/Sm (3 to 4.5), and a broad range of Yb/Sm (from 0.35 to 0.8), and partly overlaps the field of highly scavenged south Pacific clay (Plank and Langmuir, 1998; Woodhead et al., 1998; Pearce et al., 1999).

Caribbean Late Cretaceous pelagic sediment

Mid- to Late Cretaceous Caribbean pelagic sediment contains higher proportions of calcareous clay and claystone, and correspondingly lower proportions of silica, compared with Jurassic chert, reflecting a global shift from radiolarian- to foraminifera-dominated pelagic assemblages during that interval (Montgomery et al., 1994a). On-shore exposures of Late Cretaceous pelagic strata in Puerto Rico are heavily contaminated with arc-related detritus, including lenses of sandstone and ash-fall tuff, due to proximity to the Antilles arc platform, and therefore do not represent compositions of subducted sediment from the Caribbean Plate. Instead, Caribbean Cretaceous pelagic sediment is represented (Tables 8 and 9) by pelagic sediment from the Sierra de Bahoruco region of southern Hispaniola, which was obducted northward from the central Caribbean Basin onto older arc-bearing terranes during Tertiary time (Lewis and Draper, 1990; Mann et al., 1991). In particular, full analytical data for six samples of calcareous claystone from the Río Arriba Formation, consisting of over 500m of Albian to Maastrichtian chert, pelagic limestone, and claystone (Llinas, 1972) are given in Electronic Appendix Tables VIII and IX. These six samples from Hispaniola are tentatively regarded as being representative of Late Cretaceous Caribbean pelagic sediments. However, it is evident that given the small number of samples and the limited geographic distribution, additional analyses are necessary to establish a statistically more representative Caribbean Cretaceous pelagic sediment average.

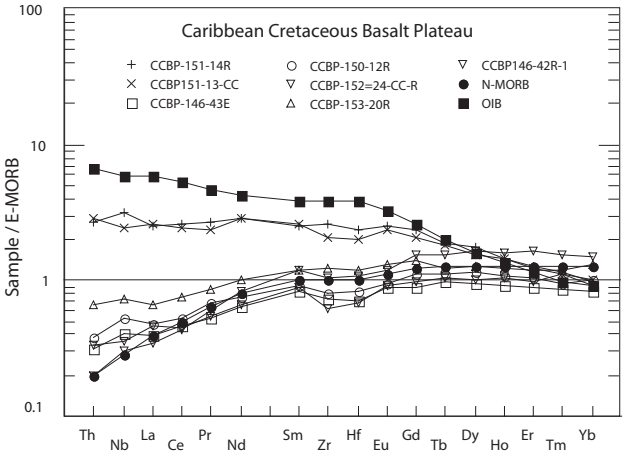

FIGURE 4 | **E-MORB-normalized incompatible element patterns of Caribbean Cretaceous Basalt Plateau. See Figure 1A for site locations.**

Distinguishing geochemical features of Atlantic and Caribbean Cretaceous pelagic sediments, and Jurassic to Early Cretaceous pelagic chert

Mesozoic pelagic sediments typically form broad positive fields sub-parallel to 1:1 MORB and OIB vectors in La-Yb element-element diagrams (Electronic Appendix Fig. II). Atlantic Cretaceous pelagic sediment distribution is subdivided into two sub-fields, one consisting predominantly of calcareous claystone and limestone and another of claystone. Slopes of both fields (La/Yb=15) are similar to Caribbean Cretaceous pelagic sediment (La/Yb=16), but this has much lower La abundances (ranging from 15 to 35 compared with 25 to 65).

Both Atlantic and Caribbean Cretaceous pelagic sediments have shallow curvilinear shapes with strongly enriched LREE segments in chondrite-normalized diagrams (Fig. 5), broadly similar to modern authigenic pelagic sediments (Taylor and McLennan, 1985). The Atlantic Cretaceous pelagic sediment pattern overlaps Pacific average authigenic sediment (Ben Othman et al., 1989) and is similar to Atlantic authigenic pelagic sediment (White et al., 1985; White and Dupré, 1986; Davidson, 1987), while Caribbean Cretaceous pelagic sediment more closely resembles south Pacific sediment.

ANALYTICAL DATA AND GEOCHEMICAL PARAMETERS

Major element Inductively-Coupled Plasma-Emission Spectrometry (ICP-ES) and trace element Inductively Coupled Plasma-Mass Spectrometry (ICP-MS) analyses reported here were performed at Acme Analytical Laboratories, Vancouver, Canada. Duplicate analyses reveal precision is within 1 to 5% of the amount present for most trace elements. Isotopic analyses were carried out by Alan P. Dickin (Jolly et al., 2007, 2008b). Samples analyzed for isotopes were leached overnight in warm diluted HCl to minimize effects of low-temperature alteration. Analytical techniques and precision limits are summarized elsewhere (Jolly et al., 1998a).

Mineralogical modes adopted for use in calculations discussed subsequently, representing a spinel lherzolite N-MORB source (fertile MORB mantle) of Pearce and Parkinson (1993), include 57.5% olivine (ol), 27.0% orthopyroxene (opx), 12.5% clinopyroxene (cpx), and 2.0% spinel. It is inferred that phases disappear from the source at constant rates during melting, and that orthopyroxene melts incongruently to olivine during early stages of fusion. Rates of phase disappearance adopted include clinopiroxene, 25% (McKenzie and O'Nions, 1991); ortopiroxene, 40% Al-spinel, 80% (Pearce and Parkinson, 1993). Mineral modes of residua from melting of spinel lherzolite are similar to ranges discussed by Pearce and Parkinson (1993). The trace element composition of fertile MORB mantle and mineral/melt trace element partition coefficients (D-values) for mantle melts are adopted from Bédard (1999). Mineral/melt partition coefficients for fractional crystallization of basalts are from Jenner et al. (1991).

PETROGENESIS OF ISLAND ARC MAGMAS, WESTERN PUERTO RICO

Major element distribution

Overlying the pre-arc basement complex of western Puerto Rico is a thick sequence of island arc rocks that decrease in age from Santonian in the southwest to mid-Eocene (~85 to 45Ma) in the northeast. The entire island arc sequence of western Puerto Rico displays a wide range of major element compositions broadly similar to global series from island arc settings, ranging from mafic basalts with low SiO_2 (<46%) to siliceous rhyolites with over 72% SiO_2, reflecting subvolcanic fractional crystallization of parental magmas (Fig. 6). The earliest of these units, and which are discussed in this report, include the prominent Boquerón (Santonian), Lajas (Santonian), and Río Loco (Early Campanian) formations (Electronic Appendix Table X). Individual units within this broad western Puerto Rico sequence have more limited compositional ranges, such that Río Loco lavas and associated rocks (Slodowski, 1956; Mattson, 1960; Krushensky and Monroe, 1978; Volckmann, 1984c) have between 6 and 13% MgO, compared to much lower values in the Boquerón-Lajas suite ranging from less than 1 to almost 5% (Fig. 6A). Silica content of Río Loco lavas, however, stands out distinctly from other members of the western Puerto Rico arc assemblage. Although MgO concentrations for most of the rocks have a normal range for basaltic mantle melts, Río Loco samples have anomalous, elevated andesitic SiO_2, ranging from 55 to over 60% (Fig. 6A), and have been recognized as being high-Mg andesites (Jolly et al., 2007). These compositions are sufficient to

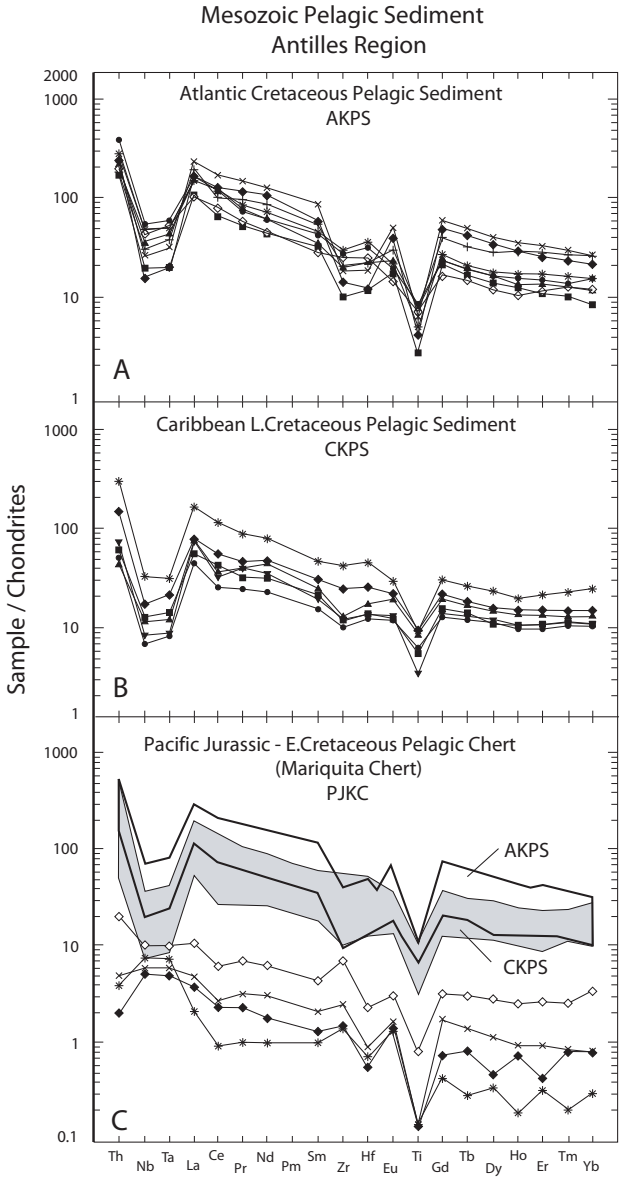

FIGURE 5 | **Chondrite-normalized incompatible element patterns of Mesozoic pelagic sediments, Antilles region. A) Atlantic Cretaceous pelagic sediment (AKPS); B) Caribbean Cretaceous pelagic sediment (CKPS); C) Pacific Jurassic-Cretaecous pelagic chert (PJKC).**

trigger a characteristic two-pyroxene-bearing, bronzite (opx) + ferroaugite (cpx) phenocryst assemblage for the Río Loco. Compositional differences reveal a consistent 19% SiO_2 surplus in average Río Loco lava (57.4% SiO_2) relative to typical mantle basalts of similar MgO content. Conversely, other major elements (including Al_2O_3, CaO, Fe_2O_3t, and TiO_2), are systematically depleted by approximately 30% (29, 30, 31, and 29%, respectively; Fig. 6B-E).

Consistent geochemical variations preclude silica enrichment through shallow crustal contamination. Instead, the observed distribution is consistent with north-dipping subduction of a ~300m thick section of Jurassic and Early Cretaceous pelagic chert (Mariquita Chert, SiO_2=86 to ~100%, Electronic Appendix Table VIII)) together with a significant complement of Late Cretaceous clay and calcareous limestones (Caribbean Cretaceous pelagic sediment) of mantle wedge source. Compositional contrasts are inferred to arise from phase transformations produced in the mantle by equilibration with an influx of siliceous melt (*i.e.*, forsterite + quartz = 2enstatite). This process enhances modal orthopyroxene in the source at the expense of olivine (ol), and dramatically alters melting patterns, leading to silica-enrichment of both melts and residua.

Except for the Río Loco Lava itself, a series of small, presumably correlative two-pyroxene basalt stocks reported by Mattson (1960) in Sierra Bermeja, and a few isolated outcrops, ranging in age from Campanian to Eocene, reported by Krushensky and Monroe (1978) from elsewhere in the volcanic sequence, silica enriched mafic compositions are rare in western Puerto Rico. Their scarcity implies special circumstances were required to incorporate subducted chert into mantle melts, as might be expected in view of extremely elevated melting points of relatively pure silica, even when wet (>1700°C, $P_{total}=P_{H2O}$). It is inferred that the high buoyancy of Mariquita chert, compared with more mafic compositions, promoted turbulent flow in the mantle wedge during initial stages of subduction, leading to isolation and fragmentation of quartz-rich mantle domains. This issue is discussed in more detail elsewhere (Jolly et al., 2007).

Multiple component mixing models

Dominance of N-MORB-type tholeiites in the western Puerto Rico pre-arc basement overlain by geochemically enriched island arc strata indicates the mantle wedge was originally comprised of fertile MORB mantle-type material, or more probably of residue from a fertile MORB mantle-type source during plate formation. Consistent with this idea, Jolly et al. (2007) proposed the development of a north-dipping island arc whose source magmas in

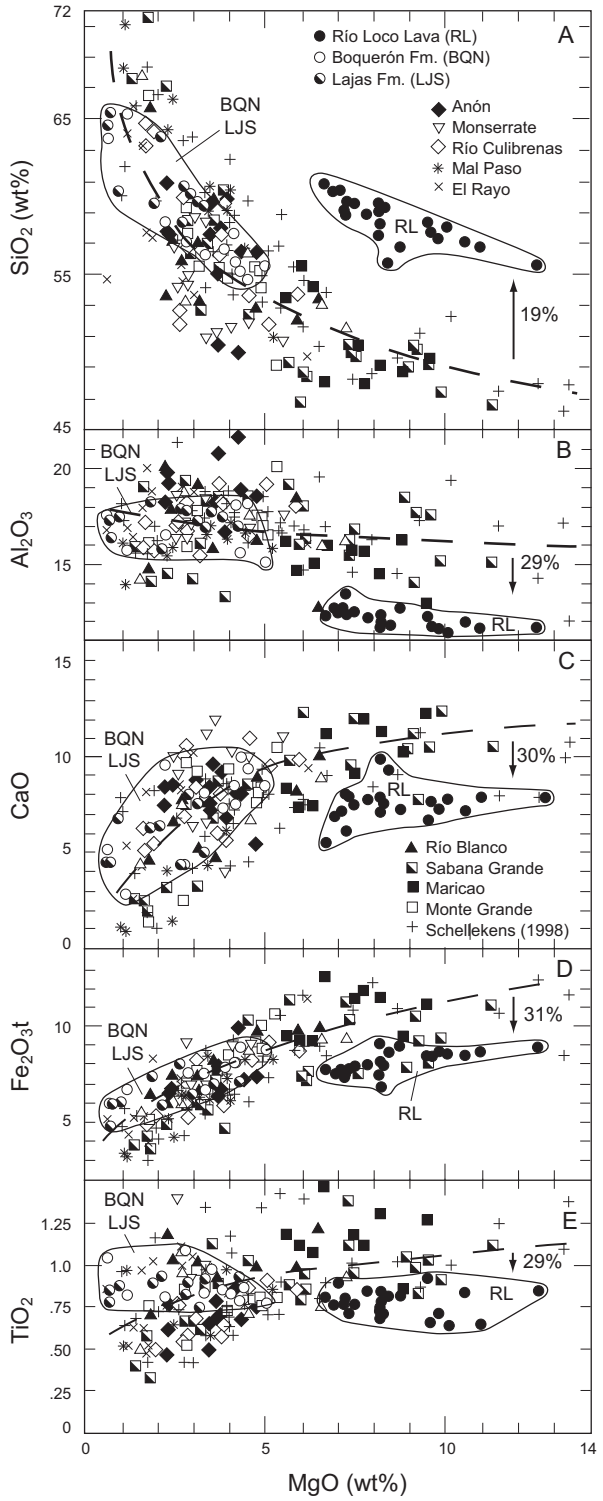

FIGURE 6 | **Major element distribution in Western Puerto Rico island arc basalt. Covariation of MgO (weight percent) and other major elements in Western Puerto Rico lavas: A) SiO_2, B) Al_2O_3, C) CaO, D) total Fe as Fe_2O_3t, and E) TiO_2. Main trends are indicated by dashed curves; fields of earliest units include Río Loco Lava (RL), and Boquerón-Lajas Fms (BQN-LJS) and are outlined. With respect to MgO, SiO_2 is enriched by 19%, while other major oxides are consistently depleted by approximately 30% in Río Loco lavas (high-Mg of Jolly et al., 2007). Deviations are consistent with incorporation of subducted Mariquita Chert (Appendix Table 8) rather than crustal assimilation. For stratigraphic succession of volcanic units see Jolly et al. (1998b, 2007).**

the mantle wedge incorporated an Atlantic Cretaceous pelagic sediment component. However, concentrations of distinctly incompatible elements (such as the LREE La, Fig. 7) in early IAB more closely correspond to Caribbean Cretaceous pelagic sediment than to Atlantic Cretaceous pelagic sediment, suggesting that the latter played only an insignificant role as a subduction component in western Puerto Rico. Moreover, incompatible element ratios of early island arc strata, including La/Nb vs Nb/Zr (Fig. 8) and Sm/Yb vs Zr/Sm (Fig. 9) are mainly intermediate between OIB and Caribbean pelagic sediments, indicating an enriched mantle source composition modified by a Caribbean Cretaceous pelagic sediment component. Geochemical trends thus favor incorporation of Caribbean Cretaceous pelagic sediment, which has lower, more appropriate trace element concentrations. Hence, geochemical relations support a tectonic model involving north-dipping subduction of the Caribbean basin involving a Caribbean Cretaceous pelagic sediment component, and establishment of a younger western Puerto Rico arc within the broad back-arc region of the older south-dipping central Puerto Rico arc.

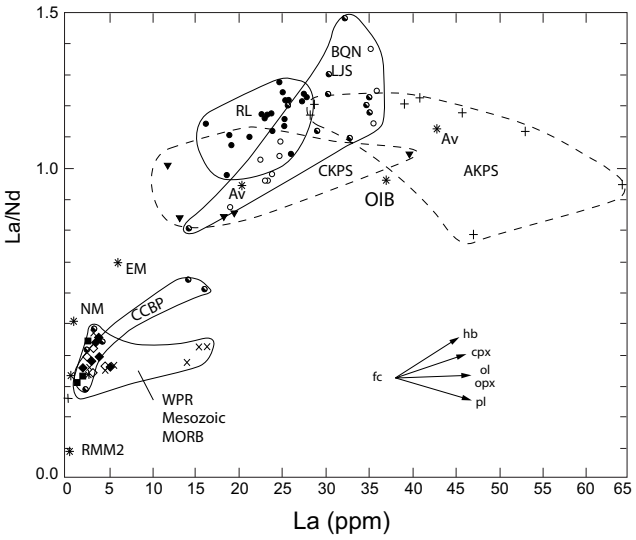

FIGURE 7 | **Trace element ratios in Western Puerto Rico (WPR). La and La/Nd. Distribution of LREE is controlled by fractional crystallization, which produces slight rightward deflection of fields, and by contaminating pelagic sediment.**

In support of this tectonic scenario is a detailed evaluation of several multiple component-mixing models that utilize OIB and Caribbean Cretaceous pelagic sediment as end members. Mineralogical modes (discussed previously) of lithospheric back-arc material are potentially highly variable due to a combination of depletion by high-degree decompression melting during plate formation and enrichment by introduction of low-degree silicate melts generated by pressure release melting as mantle material is drawn up into the melting zone (Arculus and Powell, 1986; McCulloch and Gamble, 1991). Simplified multiple component melting models are constructed from four basic modal compositions, representing variably depleted variants of a fertile MORB mantle-type spinel peridotite source, including RMM2, RMM10, RMM15, and RMM20 (Fig. 8, 9) where RMM2 represents, for example, residual MORB mantle depleted by 2% melt extraction. From each of these basic sources a further series of incompatible element-enriched starting compositions is calculated by combining various proportions (0.05, 0.02, 0.06, 0.10) of OIB (mixes denoted RMM2OIB10; RMM2OIB6 (Fig. 8, 9)). To simplify models further, calculations neglect changes in modal source composition due to addition of chert or of low-degree melt, the latter of which potentially reverses modal depletion from earlier melting events (Boudinier et al., 1988). Degree of melting in enriched sources is difficult to estimate, because Yb concentrations in depleted sources is elevated by minute proportions of OIB. To provide results comparable with central Puerto Rico and northeast Puerto Rico (Jolly et al., 2008a), melting factors are maintained at f=0.25 in figures 8 and 9; models involving other reasonable melting parameters produce similar results.

Compositions of sources derived from a given residual MORB mantle (RMM) source are distributed along the mantle line proportionally between fertile MORB mantle and OIB, such that systematic variations provide limits on mantle compositions and sediment proportions involved in production of western Puerto Rico IAB. Spacing between various source combinations depends not only on proportions of OIB added, but also on, at least, two further factors, including degree of incompatibility of a given element (Nb, for instance, is more depleted in residual sources than Zr and therefore is more sensitive to addition of small proportions of OIB), and to the degree of depletion of the starting composition (smaller proportions of sediment are required to change RMM15 or RMM20 compared with RMM2 or RMM10, for example). Lengths of melting vectors depend not only on proportion of appropriate sediment added to a mix, but also on proximity of the pelagic sediment field to the mantle trend. In La/Nb-Nb/Zr plots, lengths of vectors produced are inversely proportional to OIB, such that the addition of 10% Caribbean Cretaceous pelagic sediment to RMM2OIB2 produces a mixing line four times longer than an identical sediment proportion produces in RMM2OIB10 (Fig. 8). In Sm/Yb plots (Fig. 9) minimum vector lengths are produced by moderate proportions of OIB.

Due to the excessive number of variables involved in melting models, including degree of source depletion and proportions of both OIB and Caribbean Cretaceous pelagic sediment, estimates of sediment proportions in western Puerto Rico IAB are poorly constrained. However, analysis of melting trends for combinations of key elemental ratios provides considerable insight into the degree of source

depletion and proportions of OIB-type component. Results for highly incompatible trace elements (La/Nb-Nb/Zr, Fig. 8), for example, reveal melting vectors from RMM2 sources with appropriate Nb/Zr (~0.15) are not long enough to track across western Puerto Rico IAB fields (Fig. 8A), while all melts from sources >RMM10 have suitable OIB-like Nb/Zr (Fig. 8B-D). Other constraints are provided by moderately incompatible elements (Sm/Yb-Zr/Sm, Fig. 9),

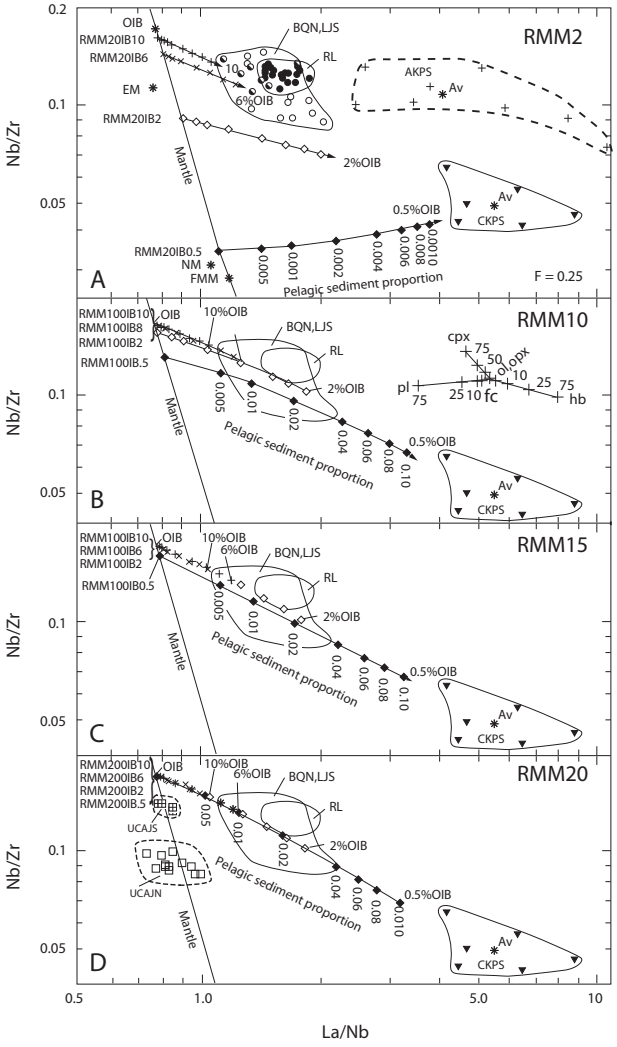

FIGURE 8 | **Multiple component melting models for La/Nb—Nb/Zr reveal extremely depleted mantle sources enriched by small proportions of both OIB-like and pelagic sediment components are required to produce WPR IAB. A) Calculated spinel peridotite sources (RMM20IB0.5, RMM20IB2, RMM20IB6, RMM20IB10), composed of RMM2 combined with various proportions of OIB (0.5, 2, 6, 10%), are aligned along the mantle trend. Fusion (f=0.25) of these sources mixed with various proportions (0.005, 0.01, 0.02, 0.04, 0.06, 0.08, 0.10) of CKPS produces melting vectors of variable lengths, depleted sources giving rise to longer vectors than enriched ones. Vectors from sources with 6 and 10% OIB have appropriate Nb/Zr to track across WPR lava fields, but these vectors indicate unlikely sediment proportions (>>10%). B) As in A, RMM10 starting source composition. C) RMM15-type starting composition. D) RMM20-type starting composition. B-D reveal sources more depleted than RMMN10 and with less than 2% OIB are required to produce melting vectors tracking across the Western Puerto Rico IAB field.**

which reveal only depleted sources (RMM15 to RMM20) with small OIB-type components (~2%) have sufficiently high Sm/Yb to produce melting vectors that intersect western Puerto Rico IAB fields.

Isotope geochemistry and isotope mixing model

Sr, Nd, and Pb isotope ratios of pre-arc and early island arc lavas of western Puerto Rico are summarized in Appendix Tables 4 and 6. Initial Sr-isotope ratios of the pre-arc basement units (Las Palmas amphibolite, Lower Cajul Formation, and Upper Cajul Formation), in particular, are displaced toward higher radiogenic compositions relative to the mantle array of Figure 10. Furthermore, ε_{Nd} values are more enriched in the Upper Cajul rocks than in the Las Palmas and Lower Cajul units. The two early island arc units (Boquerón and Río Loco) display behavior similar to the Upper Cajul in showing modest enrichment in both $(i)^{87}Sr/^{86}Sr$ and ε_{Nd}. The scatter displayed in these Sr and Nd isotope ratios are probably real and give a fairly realistic picture of the genesis of these western Puerto Rico lavas and their complex origin which, as previously discussed, are apparently dominated by a Caribbean Cretaceous pelagic sediment component, sediment component, (shown in Figure 10 and sediment isotope data summarized in Electronic Appendix Table IX). These Caribbean sediments are enriched in $(i)^{87}Sr/^{86}Sr$ and ε_{Nd}, as well as in $^{207}Pb/^{204}Pb$ and $^{208}Pb/^{204}Pb$ relative to the pre-arc and island-arc strata of western Puerto Rico, but to a much lesser extent than are Atlantic Cretaceous pelagic sediments (compare Electronic Appendix Table IX and Jolly et al., 2006, 2007). Sub-parallel fields between the Boquerón basalt and the Caribbean Cretaceous pelagic sediment suggest a possible mixing relationship. Accordingly, an isotope mixing line (Langmuir et al., 1978) has been calculated between the least radiogenic early arc Boquerón lava and the most radiogenic Caribbean Cretaceous pelagic sediment sample (Fig. 10). These results are consistent with the previously discussed trace element mixing data that Caribbean Cretaceous pelagic sediment is a likely sediment contaminant of the early arc lavas. Of course, these Sr and Nd isotope variations do not prove that the early arc lavas are solely the result of Caribbean Cretaceous pelagic sediment contamination, as some compositional input of an enriched mantle source (OIB component) may be involved, along with a possible Sr isotope spike from slab-derived fluids that displaced the Sr isotope ratios to higher values. Notably, however, these data stand in strong contrast to central Puerto Rico data correlations (Jolly et al., 2007) that show a strong trend toward Atlantic Cretaceous pelagic sediment.

TECTONIC IMPLICATIONS

Arc basalts in central Puerto Rico and northeast Puerto Rico (Jolly et al., 2006, 2008a) have prominent incompatible

trace element features resembling the signature of pelagic sediments, including 1) variably fractionated chondrite-normalized distribution patterns with elevated LREE and Th abundances, 2) flat HREE segments compared with low HREE compared with N-MORB, and 3) MORB-like HFSE (high field strength elements) abundances with deep negative Nb-Ta and Ti anomalies. Consequently, members of the central Puerto Rico and northeast Puerto Rico suites have trace element abundances intermediate between MORB and Atlantic Cretaceous pelagic sediment. Normalized patterns, for most elements, are reproduced by models involving fusion (f=0.25) of an RMM2-type spinel peridotite source contaminated with various proportions of Atlantic Cretaceous pelagic sediment. Lower trace element concentrations make Caribbean Cretaceous pelagic sediment less attractive as a potential contaminant for central Puerto Rico and northeast Puerto Rico, because excessive proportions (>>10%) are required. Hence, available data are consistent with the incorporation of a sediment component through south-dipping subduction of the North Atlantic basin.

Anomalously high Sm/Yb and Zr/Sm and low La/Sm in central Puerto Rico basalts reflect the presence of a distinct, low-Zr/Sm slab-derived basaltic component in addition to Atlantic Cretaceous pelagic sediment. Candidates include low-degree basalt melt generated from a wide variety of potential sources within the subducted oceanic crust, such as partly eclogized hornblende gabbro of accumulate (low-Zr/Sm) origin. The question of how amphibolite-bearing material is preserved to sufficient depths within the subducted slab to reach melting temperatures is the subject of considerable debate (Defant and Drummond, 1990; Defant et al., 1991; Elthon, 1991; Drummond et al., 1996; Bédard, 1999). Presumably in central Puerto Rico, coarse-grained, low-melting gabbroic accumulates within the descending oceanic slab retained adequate hornblende to promote fusion at some stage of subduction. Sediment: slab melt ratios tended to rise throughout volcanism, from 1:2 in early volcanic phases I and II, to between 1:1 and 1:0 in phases III and IV. Trends are consistent with progressively decreasing temperatures in the slab, as outlined in the models of Peacock (Peacock, 1993; Peacock et al., 1994), and with a concurrent decrease in slab melt proportion. The decline in basaltic slab melt was accompanied by increasing sediment proportions, from moderate levels between 0.5-2% during phases I and II to extremely elevated concentrations exceeding 5% during phases III and IV. Consequently, proportions of basaltic slab melt and Atlantic Cretaceous pelagic sediment are roughly inversely proportional. Unusually high sediment proportions in later volcanic phases compared with modern arc systems are inferred to arise from subduction of a progressively thickening sediment pile. Introduction of a significant OIB-type component into the central Puerto Rico mantle wedge source at any stage is precluded by the high magnitude of negative Nb-anomalies.

In marked contrast with central Puerto Rico, trace element abundances in western Puerto Rico IAB more closely resemble OIB than N-MORB. Significantly, Atlantic Cretaceous pelagic sediment is excluded as a possible component in western Puerto Rico by elevated abundances of many more incompatible elements, which exceed concentrations in OIB. Instead, the rocks have trace element ratios intermediate between Caribbean Cretaceous pelagic sediment and OIB, consistent with north-dipping subduction of the Caribbean Basin. Accordingly, although sediment proportions are poorly constrained due to an

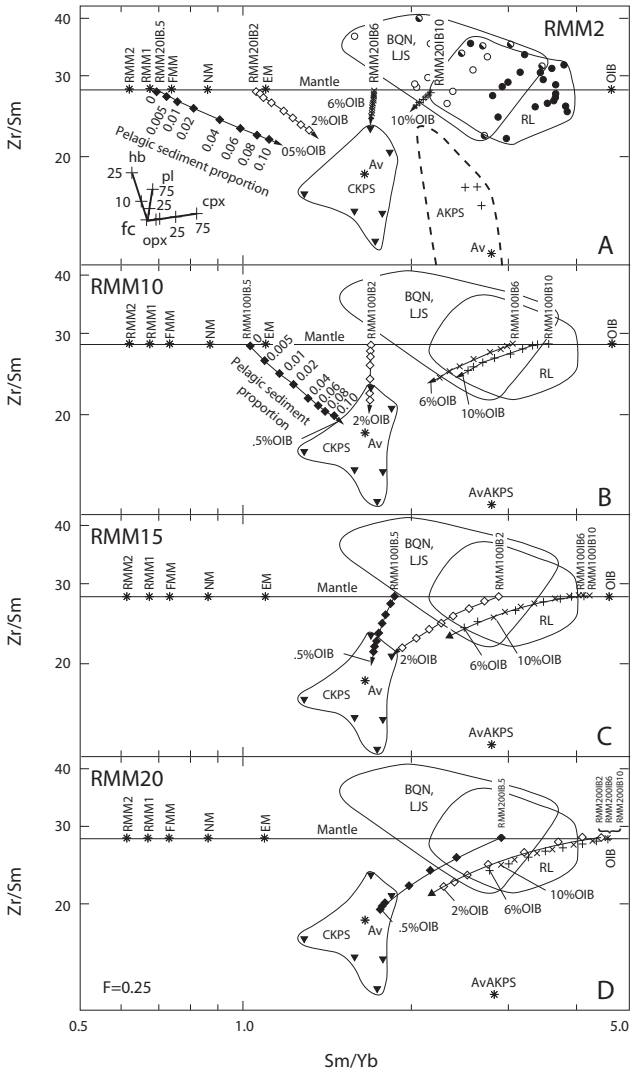

FIGURE 9 | **Multiple component melting models for Sm/Yb-Zr/Sm further constrain suitable source compositions in Western Puerto Rico. Suitable melting vectors tracking across WPR lava fields (<5% CKPS) are produced only by highly depleted sources (RMM15 TO RMM20) mixed with small proportions of IOB (0.5 to 2%) as in Figure 8; symbols and parameters as in Figure 8.**

excessive number of variables, multiple component melting models (f=0.25) generate suitable melting vectors that track across the western Puerto Rico IAB fields on variation diagrams (Fig. 8, 9). The most appropriate models involve fusion of highly depleted spinel peridotite (RMM15 to RMM20), lightly overprinted by addition of a small OIB-type component (up to 2%), and mixed with various proportions of Caribbean Cretaceous pelagic sediment. The occurrence of anomalous, SiO_2-enriched, two-pyroxene-bearing basalt in the western Puerto Rico assemblage, apparently generated by incorporation of subducted Jurassic Mariquita Chert of Pacific (Farallon) origin, is also consistent with tectonic models involving north-dipping subduction.

The geographic position of the second, north-dipping western Puerto Rico subduction zone within the broad back-arc region of the original south-dipping Antillean arc system leads naturally to the conclusion that enrichment of the western Puerto Rico mantle source occurred through variable veining of lithosphere by low-degree, decompression melts associated with back-arc counter-flow in the older arc. Accordingly, it is inferred that small proportions of OIB-like, low-degree basalt melt were added to back-arc lithospheric mantle peridotite that had already been strongly depleted during original plate formation. The overprinted lithosphere, representing a back-arc upper mantle enrichment zone, was subsequently sampled by the younger (~85Ma) western Puerto Rico arc.

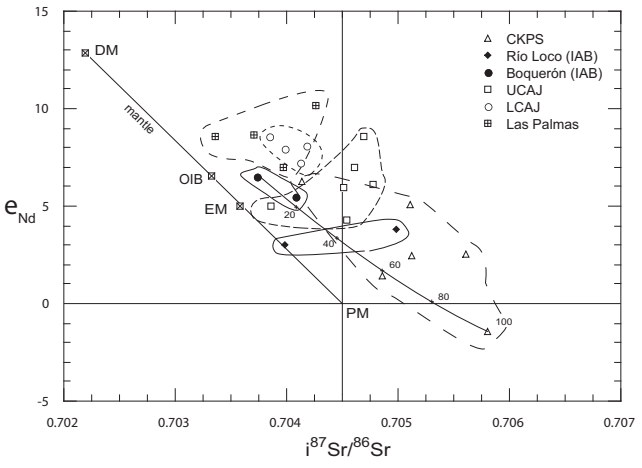

FIGURE 10 | **Sr- and Nd-isotope ratios of pre-arc basement and early island arc lavas of WPR. Representative mantle array from Hart (1988) and Rollinson (1993). Pre-arc basement complex includes MORB tholeiites from the Jurassic Lower Cajul Formation (LCAJ), related Las Palmas amphibolite, and plateau basalts from the Upper Cajul Formation (UCAJ); early island arc lavas are from the Boquerón and Río Loco formations; CKPS represents Caribbean Cretaceous pelagic sediments.**

CONCLUSIONS

In this paper we present an overview of the pre-arc basement complex of southwestern Puerto Rico, summarize the geological and geochemical characteristics of the basement complex, and discuss the geochemical and tectonic evolution of the early island arc basaltic rocks in western Puerto Rico that overlie the pre-arc complex, utilizing major element, trace element, and Sr, Nd, and Pb isotope ratio data. The incompatible element distribution and multiple component fractional mixing models presented here, based on fusion of modified fertile MORB mantle-type mantle sources, are consistent with the following conclusions:

Incompatible trace element abundances of island arc strata in western Puerto Rico (~85 to 45Ma) are intermediate between OIB and pelagic sediments, indicating the rocks were derived from a highly enriched mantle source with OIB-like compositions.

Enriched incompatible element abundances in western Puerto Rico IAB, equal to or higher than OIB, preclude Atlantic Cretaceous pelagic sediment as a possible component, but are consistent with the incorporation of Caribbean Cretaceous pelagic sediment, and with north-dipping subduction of the Caribbean Basin. Elevated SiO_2, which triggered a two-pyroxene phenocryst mineralogy in certain early western Puerto Rico arc lavas, is consistent with incorporation of subducted chert, represented in the western Puerto Rico basement by Mariquita Chert of Jurassic Pacific (Farallon) provenance.

Multiple component mixing models reveal that shallow negative Nb- and slighty positive Zr-Hf-normalized anomalies and elevated Nb/Zr in western Puerto Rico IAB reflect the presence, in addition to Caribbean Cretaceous pelagic sediment, of a small OIB-type source component (up to ~2%) superimposed on a highly depleted (RMM15 to RMM20) mantle residuum.

The western Puerto Rico arc system (dating from ~85Ma) developed within and sampled lithospheric material from the back-arc upper mantle enrichment zone associated with the older, south-dipping central Puerto Rico arc (from ~125Ma).

The data on which this paper is based is presented in an online appendix (Tables 1-10) that includes both the pre-arc basement complex and the overlying early island arc sequence.

ACKNOWLEDGMENTS

The authors acknowledge with gratitude the constructive reviews of John F. Lewis and J. A. Proenza whose comments and suggestions greatly improved the manuscript.

REFERENCES

Arculus, R.J., Powell, R., 1986. Source component mixing in the regions of arc magma generation. Journal of Geophysical Research, 91, 5913-5926.

Bédard, J.H., 1999. Petrogenesis of boninites from the Betts Cove Ophiolite, Newfoundland, Canada: Identification of subducted source components. Journal of Petrology, 40, 1853-1889.

Ben Othman, D., White, W.M., Patchett, J., 1989. The geochemistry of marine sediments, island arc magma genesis, and crust-mantle recycling. Earth and Planetary Science Letters, 94, 1-21.

Boudinier, J.L., Dupuy, C., Dostal, J., 1988. Geochemistry and petrogenesis of eastern Pyrenean peridotites. Geochimica et Cosmochimica Acta, 52, 2893-2907.

Curet, A.F., 1986. Geologic map of the Mayagüez and Rosario quadrangles. Puerto Rico. U.S. Geological Survey Miscellaneous Investigations Map, I-1657, scale 1:20,000.

Davidson, J.P., 1987. Crustal contamination *versus* subduction zone enrichment: Examples from the Lesser Antilles and implications for mantle source compositions of island arc volcanic rocks. Geochimica et Cosmochimica Acta, 51, 2185-2198.

Defant, M.J., Drummond, M.S., 1990. Derivation of some modern arc magmas by melting of young subducted lithosphere. Nature, 347, 662-665.

Defant, M.J., Richardson, P.M., De Boer, J.Z., Stewart, R.H., Maury, R.C., Bellon, H., Drummond, M.S., Feigenson, M.D., Jackson, T.E., 1991. Dacite genesis via both slab melting and differentiation: Petrogenesis of La Yeguada volcanic complex, Panama. Journal of Petrology, 32, 1101-1142.

Donnelly, T.W., 1989. Geologic history of the Caribbean and Central America. In: Bally, A.W., Palmer, A.R. (eds.). The Geology of North America-An overview. Boulder (Colorado), Geological Society of America, A, 299-321.

Donnelly, T.W., 1994. The Caribbean Cretaceous basalt association: A vast igneous province that includes the Nicoya complex of Costa Rica. In: Seyfried, H., Hellman, W. (eds.). Geology of an Evolving Island Arc: The Isthmus of Southern Nicaragua, Costa Rica, and Western Panama: Stuttgart, Germany, Profile (Band 7). Institut für Geologie und Palaontologie, 17-45.

Dosso, L., Bougault, H., Joron, J.-L., 1993. Geochemical morphology of the north mid-Atlantic Ridge, 10-24°: Trace element-isotope complementarity. Earth and Planetary Science Letters, 120, 443-462.

Draper, G., 1986. Blueschists and associated rocks in eastern Jamaica and their significance for Cretaceous plate-margin development in the northern Caribbean. Geological Society of America Bulletin, 97, 48-60.

Drummond, M.S., Defant, M.J., Kepezhinski, P.K., 1996. Petrogenesis of slab-derived trondhjemite-tonalite-dacite/adakite magmas. Transactions of the Royal Society of Edinburgh, 87, 205-215.

Elthon, D., 1991. Geochemical evidence for formation of the Bay of Islands ophiolite above a subduction zone. Nature, 354, 140-143.

García-Casco, A., Torres-Roldán, R., Millán, G., Iturralde-Vinent, M.A., Núñez Cambra, K., Lázaro Calisalvo, C., Rodríguez Vega, A., 2006. High-pressure metamorphism of ophiolites in Cuba. Geologica Acta, 4(1-2), 63-88.

Glover, L. III, 1971. Geology of the Coamo area, Puerto Rico, and its relation to the volcanic arc-trench association. U.S. Geological Survey Professional Paper, 636, Washington, D. C., 102pp.

Hart, S.R., 1988. Heterogeneous mantle domains: signatures, genesis and mixing chronologies. Earth and Planetary Science Letters, 90, 273-296.

Hauff, F., Hoernle, K., Schminke, H.-U., Werner, R., 1997. A Mid Cretaceous origin for the Galapagos hotspot: Volcanological, petrological and geochemical evidence from Costa Rican oceanic crustal segments. Geologische Rundschau, 86, 141-155.

Hauff, F., Hoernle, K., Tilton, G., Graham, D.W., Kerr, A.C., 2000. Large volume recycling of oceanic lithosphere over short time scales: geochemical constraints from the Caribbean Large Igneous Province. Earth and Planetary Science Letters, 174, 247-263.

Iturralde-Vinent, M.A., 1998. Synopsis of the geological constitution of Cuba. Acta Geologica Hispanica, 33, 9-56.

Jahn, B., Bernard-Griffiths, J., Charlot, R., Cornichet, J., Vidal, F., 1980. Nd and Sr isotopic composition and REE abundances of Cretaceous MORB (holes 417D and 418A, legs 51, 52, and 53). Earth and Planetary Science Letters, 48, 171-184.

Jansma, P., Mattioli, G., López, A., DeMets, C., Dixon, T., Mann, P., Calais, E., 2000. Neotectonics of Puerto Rico and the Virgin Islands, northeastern Caribbean, from GPS geodesy. Tectonics, 19, 1021-1037.

Jenner, G.A., Dunning, G.R., Malpas, J., Brown, M., Bruce, T., 1991. Bay of Islands and Little Port complex, revisited: age, geochemical and isotope evidence confirm suprasubduction zone origin. Canadian Journal of Earth Sciences, 28, 1635-1652.

Jolly, W.T., Lidiak, E.G., Dickin, A.P., 2006. Cretaceous to Mid-Eocene pelagic sediment budget in Puerto Rico and the Virgin Islands (northeast Antilles island arc). Geologica Acta, 4(1-2), 35-62.

Jolly, W.T., Lidiak, E.G., Dickin, A.P., 2008a. Bimodal volcanism in northeast Puerto Rico and the Virgin Islands (Greater Antilles Island Arc): Genetic links with Cretaceous subduction of the mid-Atlantic ridge Caribbean spur. Lithos, 103, 393-414.

Jolly, W.T., Lidiak, E.G., Dickin, A.P., 2008b. The case for persistent southwest-dipping Cretaceous convergence in the northeast Antilles: Geochemistry, melting models, and tectonic implications. Geological Society of America Bulletin, 120, 1036-1052.

Jolly, W.T., Lidiak, E.G., Dickin, A.P., Wu, T.-W., 1998a. Geochemical diversity of Mesozoic island arc tectonic blocks in eastern Puerto Rico. In: Lidiak, E.G., Larue, D.K. (eds.). Tectonics and Geochemistry of the Northeastern Caribbean. Boulder (Colorado), Geological Society of America, 322 (Special Paper), 67-98.

Jolly, W.T., Lidiak, E.G., Schellekens, J.H., Santos, H., 1998b. Volcanism, tectonics, and stratigraphic correlations in Puerto Rico. In: Lidiak, E.G., Larue, D.K. (eds.). Tectonics and Geochemistry of the Northeastern Caribbean. Boulder (Colorado), Geological Society of America, 322 (Special Paper), 1-34.

Jolly, W.T., Schellekens, J.H., Dickin, A.P., 2007. High-Mg andesites and related lavas from southwest Puerto Rico (Greater Antilles Island Arc): Petrogenetic links with emplacement of the Late Cretaceous Caribbean mantle plume. Lithos, 98, 1-26.

Kerr, A.C., Tarney, J., 2005. Tectonic evolution of the Caribbean and northwestern South America: The case for accretion of two Late Cretaceous oceanic plateaus. Geology, 33, 269-272.

Kerr, A.C., Tarney, J., Kempton, P., Spadea, P., Nivia, A., Marriner, G., Duncan, R., 2002. Pervasive mantle plume head heterogeneity: Evidence from the late Cretaceous Caribbean-Colombian oceanic plateau. Journal of Geophysical Research, 107, ECV 2-1.

Krushensky, R.D., Monroe, W.H., 1978. Geologic map of the Yauco and Punta Verraco quadrangles. Puerto Rico. U.S. Geological Survey Miscellaneous Investigations Map, I-1147, scale 1:20,000.

Langmuir, C.H., Vocke, R.D.Jr., Hanson, G.N., Hart, S.R., 1978. A general mixing equation with applications to Icelandic basalts. Earth and Planetary Science Letters, 37, 380-392.

Lapierre, H., Dupuis, V., Mercier de Lepinay, B., Bosch, D., Monie, P., Tardy, M., Maury, R.C., Hernandez, J., Polve, M., Yeghicheyan, D., Cotten, J., 1999. Late Jurassic oceanic crust and Upper Cretaceous Caribbean plateau picritic basalts exposed in the Duarte Igneous Complex, Hispaniola. Journal of Geology, 107, 193-207.

Lewis, J.F., Draper, G., 1990. Geology and tectonic evolution of the northern Caribbean margin. In: Dengo, G., Case, J.E. (eds.). The Caribbean region. Boulder (Colorado), Geological Society of America, H, 77-140.

Lewis, J.F., Escuder-Viruete, J.E., Hernaiz Huerta, P.P., Gutierrez, G., Draper, G., Pérez-Estaún, A., 2002. Subdivisión geoquímica del arco isla Circum-caribeno, Cordillera Central Dominicana: Implicaciones para la formación, acreción y crecimiento cortical en un ambiente interoceánico. Acta Geológica Hispanica, 37, 81-122.

Llerandi-Roman, P.A., 2004. Geologic and Tectonic History of the Western Section of the Sabana grande Quadrangle. M.S. Thesis. Mayagüez (Puerto Rico), University of Puerto Rico, 134pp.

Llinas, R., 1972. Geologia del area Polo Duverge, Cuenca de Enriquillo. Codia, Publicación del Colegio Dominicano de Ingenieros, Arquitectos y Agrimensores, part 1(31), 55-65.

Mann, P., Draper, G., Lewis, J.F., 1991. An overview of the geologic and tectonic development of Hispaniola. In: Mann, P., Draper, G., Lewis, J.F. (ed.). Geologic and tectonic development of the North American-Caribbean plate boundary in Hispaniola. Boulder (Colorado), Geological Society of America, 262 (Special Paper), 1-28.

Marchesi, C., Garrido, C., Bosch, D., Proenza, J., Gervilla, F., Monie, P., Rodríguez-Vega, R., 2007. Geochemistry of Cretaceous magmatism in eastern Cuba: Recycling of North American continental sediments and implications for subduction polarity in the Greater Antilles paleo-arc. Journal of Petrology, 48, 1813-1840.

Martínez-Colon, M., 2003. Geologic and Tectonic History of the Eastern Section of the Sabana Grande Quadrangle. M.S. Thesis. Mayagüez (Puerto Rico), University of Puerto Rico, 104pp.

Mattson, P.H., 1960. Geology of the Mayagüez area, Puerto Rico. Geological Society of America Bulletin, 71, 319-362.

Mattson, P.H., 1979. Subduction, buoyant braking, flipping and strike-slip faulting in the northern Caribbean. Journal of Geology, 87, 293-304.

Mauffret, A., Leroy, S., 1997. Seismic stratigraphy and structure of the Caribbean igneous province. Tectonophysics, 283, 61-104.

McCulloch, M.T., Gamble, J.A., 1991. Geochemical and geodynamical constraints on subduction zone magmatism. Earth and Planetary Science Letters, 102, 358-374.

McIntyre, D.H., 1975. Geologic map of the Maricao quadrangle, western Puerto Rico. U.S. Geological Survey Miscellaneous Investigations Map, I-918, scale 1:20,000.

McKenzie, D., O'Nions, R.K., 1991. Partial melt distributions from inversion of rare earth element concentrations. Journal of Petrology, 32, 1021-1091.

Mitchell, S.F., 2006. Timing and implications of Late Cretaceous tectonic and sedimentary events in Jamaica. Geologica Acta, 4(1-2), 171-178.

Montgomery, H., Pessagno, E.A.Jr., Lewis, J.F., Schellekens, J.H., 1994a. Paleogeography of Jurassic fragments in the Caribbean. Tectonics, 13, 725-732.

Montgomery, H., Pessagno, E.A.Jr., Pindell, J.L., 1994b. A 195Ma terrane in a 165Ma sea: Pacific origin of the Caribbean plate. GSA Today, 4, 1-6.

Peacock, S., 1993. Large-scale hydration of the lithosphere above subducting slabs. Chemical Geology, 108, 49-59.

Peacock, S.M., Rushmer, T., Thompson, A.B., 1994. Partial melting of subducting oceanic crust. Earth and Planetary Science Letters, 121, 227-244.

Pearce, J.A., Kempton, P.D., Nowell, G.M., Noble, S.R., 1999. Hf-Nd element and isotope perspective on the nature and provenance of mantle and subduction components in western Pacific arc-basin systems. Journal of Petrology, 40, 1579-1611.

Pearce, J.A., Parkinson, I.J., 1993, Trace element models for mantle melting: Application to volcanic arc petrogenesis. Geological Society of London, 76 (Special Paper), 76, 373-403.

Pindell, J.L., Barrett, S.F., 1990. Geological evolution of the Caribbean region: a plate tectonic perspective. In: Dengo, G., Case, J.E. (eds.). The Caribbean Region. Boulder (Colorado), Geological Society of America, The Geology of North America, H, 405-432.

Pindell, J.L., Cande, S.C., Pitman, W.C.III, Rowley, D.B., Dewey, J.F., La Brecque, J., Haxby, W., 1988. A plate-

kinematic framework for models of Caribbean evolution. Tectonophysics, 155, 121-138.

Plank, T., Langmuir, C.H., 1998. The chemical composition of subducting sediment and its consequences for the crust and mantle. Chemical Geology, 145, 325-394.

Proenza, J.A., Díaz-Martínez, R., Marchesi, C., Melgarejo, J.C., Gervilla, F., Garrido, C.J., Rodríguez-Vega, A., Lazano-Santacruz, R., Blanco-Moreno, J.A., 2006. Primitive island-arc Cretaceous volcanic rocks in eastern Cuba: the Teneme Formation. Geologica Acta, 4(1-2), 103-122.

Rollinson, H., 1993. Using Geochemical Data: Evaluation, Presentation, Interpretation. Essex (England), Longman Scientific & Technical, 352pp.

Schellekens, J.H., 1998. Geochemical evolution and tectonic history of Puerto Rico. In: Lidiak, E.G., Larue, D.K. (eds.). Tectonics and Geochemistry of the Northeastern Caribbean. Boulder (Colorado), Geological Society of America, 322 (Special Paper), 35-66.

Schellekens, J.H., Montgomery, H., Joyce, J., Smith, A.L., 1991. Late Jurassic to late Cretaceous development of island arc crust in southwestern Puerto Rico. In: Larue, D.K., Draper, G. (eds.). 12th Caribbean Geological Conference Transactions, St. Croix, U. S. Virgin Islands, Miami Geological Society, 268-281.

Slodowski, T.R., 1956. Geology of the Yauco area, Puerto Rico. Ph. D. Thesis. Princeton (New Jersey), Princeton University, 130pp.

Sun, S.-S., McDonough, W.F., 1989. Chemical and isotopic systematics of oceanic basalts: implications for mantle composition and processes. In: Saunders, A.D., Norry, M.J. (eds.). Magmatism in the Ocean Basins. Oxford (United Kingdom), Blackwell Scientific Publications, Geological Society, 42 (Special Publications), 313-345.

Taylor, S.R., McLennan, S.M., 1985. The Continental Crust: its Composition and Evolution. Oxford, Blackwell Scientific Publications, 312pp.

Volckmann, R.P., 1984a. Geologic map of the Cabo Rojo and Parguera quadrangles, southwest Puerto Rico. U.S. Geological Survey Miscellaneous Investigations Map, I-1557, scale 1:20,000.

Volckmann, R.P., 1984b. Geologic map of the Puerto Real quadrangle, southwest Puerto Rico. U.S. Geological Survey Miscellaneous Investigations Map, I-1559, scale 1:20,000.

Volckmann, R.P., 1984c. Geologic map of the San German quadrangle, southwest Puerto Rico. U.S. Geological Survey Miscellaneous Investigations Map, I-1558, scale 1:20,000.

White, W.M., Dupré, B., 1986. Sediment subduction and magma genesis in the Lesser Antilles: Isotopic and trace element constraints. Journal of Geophysical Research, 91, 5927-5941.

White, W.M., Dupré, B., Vidal, P., 1985. Isotope and trace element geochemistry of sediments from the Barbados ridge-Demerara plain region, Atlantic Ocean. Geochimica et Cosmochimica Acta, 49, 1875-1886.

Woodhead, J.D., Eggins, S.M., Johnson, R.W., 1998. Magma genesis in the New Britain island arc: Further insights into melting and mass transfer processes. Journal of Petrology, 39, 1641-1668.

Manuscript received November 2010;
revision accepted June 2011;
published Online June 2011.

ELECTRONIC APPENDIX

Supplementary data associated with this article can be found in the online version of this manuscript.

APPENDIX TABLES

Table	Status
1) Monte del Estado Peridotite	New Data
2) Las Palmas Amphibolite	New Data
3) Lower Cajul MORB (LCAJ)	Revised Data
4) Las Palmas and LCAJ Isotopes	New and Revised
5) Upper Cajul MORB (UCAJ)	Revised Data
6) Upper Cajul MORB (UCAJ) Isotopes	Revised Data
7) Caribbean Cretaceous Basalt Plateau (CCBP)	Revised Data
8) Pelagic Sediments	New and Revised
9) Pelagic Sediments Isotopes	New and Revised
10) Early Island Arc Volcanic Rocks (WPR)	Revised Data

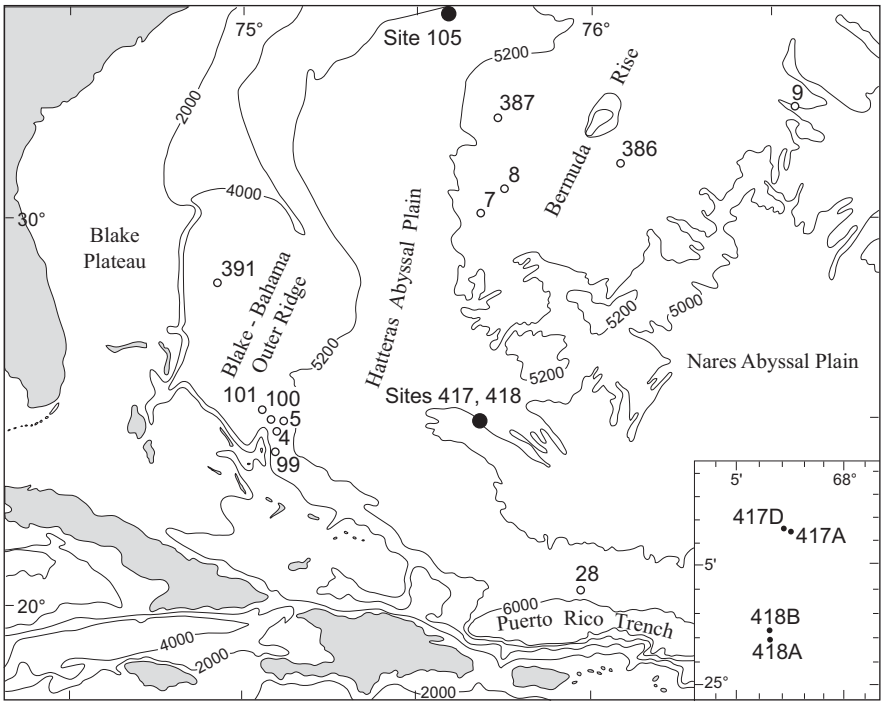

FIGURE I | **Map of southwestern North Atlantic area showing locations of DSDP drill sites, the source of analyzed samples (Table 8) of Atlantic Cretaceous pelagic sediments (AKPS).**

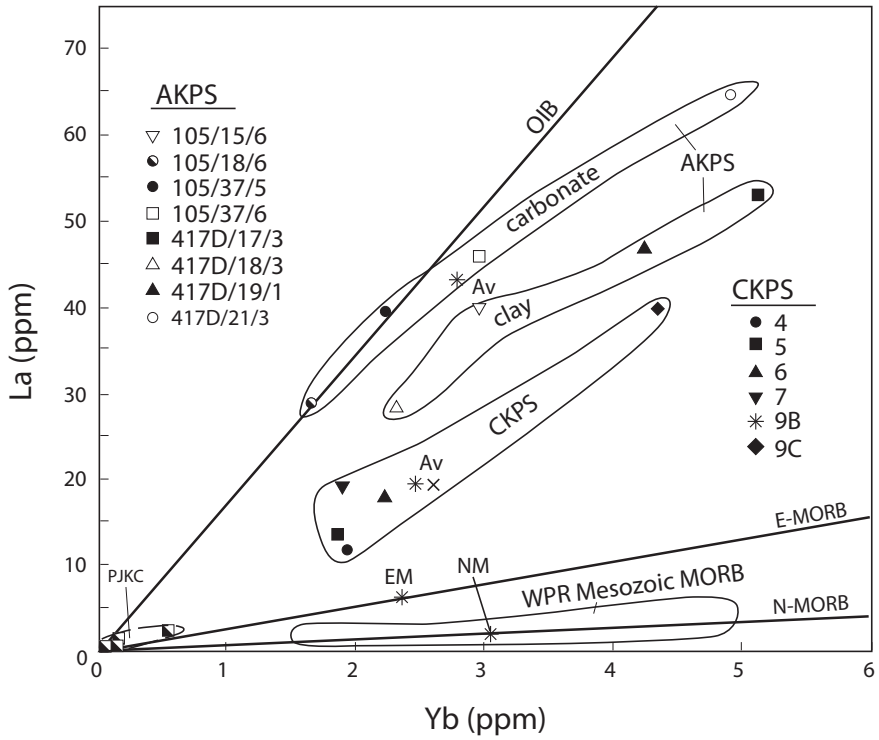

FIGURE II | **La and Yb compared to WPR Mesozoic MORB and trends of major oceanic basalt series (Sun and McDonough, 1989). AKPS forms two elongate fields sub-parallel to the OIB trend, one of carbonate with relatively high La and low Zr, and another of abyssal claystone with lower La and relatively high Zr. CKPS forms a subparallel field more depleted in La, reflecting a higher mafic volcanogenic component, as in South Pacific sediments.**

TABLE I | **Major and trace element data, Monte del Estado Serpentinized Peridotite, Puerto Rico**

Sample	001-96	002-96	012-94	014-94	017-94	021-94	30-94	32-94	37-94	50A-94	52-94	59-93	60-93	61-93	62-93	63-93	78-94	71-94	77H-94	90-93	92-94	92A-94	154-94	Avg Lherz	Avg Harz
Unit	H2	H2					H	L		L	L	L	L		L	L		H	H				H2		
SiO_2	40.18	39.45	39.82	39.30	40.33	39.73	41.28	39.64	39.82	40.83	39.52	35.02	38.19	38.38	41.23	38.42	39.24	39.86	39.50	38.89	38.72	38.64	39.88	45.43	43.73
TiO_2	0.04	0.05	0.01	0.05	0.06	0.07	0.02	0.04	0.07	0.05	0.04	0.07	0.05	0.05	0.07	0.04	0.02	0.01	0.02	0.04	0.04	0.03	0.05	0.45	0.28
Al_2O_3	1.49	1.65	1.10	1.86	2.59	2.50	0.98	2.12	2.54	1.77	2.25	2.39	2.19	1.98	2.36	1.87	1.66	1.14	1.37	1.83	1.95	1.58	1.77	4.39	2.57
Fe_2O_3	7.45	7.30	7.40	6.64	8.13	7.96	6.67	7.91	8.06	6.93	7.95	8.39	7.56	7.60	8.09	8.28	7.98	7.04	6.86	7.05	8.02	8.29	7.80	5.15	6
FeO	0.00	0.00	0.00	0.00	0.00	0.00	0.00	0.00	0.00	0.00	0.00	0.00	0.00	0.00	0.00	0.00	0.00	0.00	0.00	0.00	0.00	0.00	0.00	7.44	7.09
MnO	0.13	0.11	0.11	0.12	0.11	0.11	0.17	0.11	0.11	0.12	0.11	0.13	0.12	0.13	0.12	0.13	0.11	0.12	0.15	0.09	0.11	0.13	0.10	0.17	0.16
MgO	36.73	37.62	35.11	35.55	35.54	35.87	43.57	36.61	36.48	37.09	36.68	40.12	36.99	36.35	36.34	36.45	35.79	39.86	35.58	36.11	36.98	35.60	35.94	30.31	36.34
CaO	0.52	0.46	0.35	2.31	2.95	2.77	0.64	2.20	3.01	3.21	2.29	2.51	2.03	0.28	2.73	0.14	1.15	0.39	0.94	1.97	2.13	0.72	0.63	5.68	3.18
Na_2O	0.18	0.16	0.01	0.05	0.06	0.04	0.10	0.03	0.09	0.03	0.02	0.23	0.04	0.00	0.07	0.20	0.01	0.09	0.00	0.02	0.03	0.03	0.01	0.59	0.34
K_2O	0.01	0.00	0.00	0.00	0.00	0.00	0.00	0.00	0.00	0.00	0.00	0.01	0.00	0.00	0.00	0.01	0.00	0.00	0.00	0.00	0.00	0.00	0.00	0.27	0.15
P_2O_5	0.00	0.00	0.09	0.08	0.08	0.08	0.00	0.08	0.08	0.07	0.05	0.00	0.07	0.09	0.07	0.08	0.07	0.07	0.08	0.06	0.06	0.07	0.07	0.12	0.14
LOI	13.11	13.28	15.30	13.30	9.40	10.10	6.61	10.50	9.00	9.10	10.30	10.95	11.90	14.30	8.20	13.80	13.20	12.00	14.70	13.20	11.20	14.10	13.20	0	0
Subtotal	99.84	100.08	99.30	99.26	99.25	99.23	100.04	99.24	99.26	99.20	99.21	99.82	99.14	99.16	99.28	99.42	99.23	100.58	99.20	99.26	99.24	99.19	99.45	100.00	99.98
Cr	3282	3068			2892		3399	2700		3098	2879	2575	3069	2763	3056	2687		1809	3341				2175		
Ni	2030	1980			1912		2307	2177		1879	2046	2100	1975	1968	2022	2256		2350	2245				2021		
Ta	0	0					0.01	0		0	0	0	0	0.015	0	0.05		0.01	0.01				0.088		
Nb	0.238	0.291					0.01	0.4		0.01	0.27	0.29	0.326	0.2	0.21	0		0	0.06				0.2		
Hf	0	0.082					0	0.018		0	0.082	0.027	0.031	0	0.026	0.1		0.06	0				0		
Zr	0.281	0.17					0.27	0.19		0.2	0.888	1.258	0.888	0.537	0.962	0		1.52	0.39				1.232		
Ti	114	440					119.9	182		570	226.5	418	365	359.7	365	0		59.95	179.9				299.8		
Y	0.56	1.148					0.63	1.092		1.96	2.156	1.596	1.988	1.391	1.848	1		1	0.77				0.73		
Th	0.165	0.206					0.01	0.3		1.32	0.38	1.201	1.313	0.23	0.234	0.2		0.01	0.01				0.029		
U	2.29	0.46					0.007	0		0	0	0	0.98	0.039	0	0.1		0	0				0		
La	0.53	0.6					0.01	1.18		10.53	7.375	2.95	10	0.062	2.552	1.61		0.01	0.04				0.09		
Ce	0.6	0.7					0.02	1.112		11.25	4.275	2.925	6.66	0.1	2.52	1.78		0.04	0.07				0.297		
Pr	0.015	0.024					0	0.06		0.1	0.14	0.08	0.14	0.014	0.13	0		0.01	0.01				0.037		
Nd	0.1	0.128					0	0.15		0.21	0.205	0.19	0.41	0.1	0.35	1		0	0.07				0.188		
Sm	0.024	0.033					0	0.039		0.063	0.066	0.053	0.13	0.077	0.103	0.07		0	0.03				0.074		
Eu	0.01	0.02					0	0.018		0.046	0.049	0.033	0.044	0.022	0.037	0.02		0	0.01				0.024		
Gd	0.077	0.103					0.04	0.085		0.191	0.247	0.147	0.191	0.129	0.166	0		0	0.03				0.117		
Tb	0.011	0.021					0.01	0.019		0.04	0.046	0.03	0.04	0.027	0.033	0.04		0	0.01				0.024		
Dy	0.086	0.176					0.075	0.153		0.284	0.333	0.23	0.279	0.275	0.213	0		0.033	0.13				0.219		
Ho	0.024	0.048					0.03	0.042		0.077	0.081	0.061	0.08	0.057	0.071	0		0	0.03				0.048		
Er	0.092	0.151					0.1	0.134		0.241	0.244	0.202	0.252	0.171	0.226	0		0	0.08				0.107		
Tm	0.016	0.025					0.02	0.024		0.039	0.037	0.036	0.041	0.028	0.036	0		0	0.02				0.023		
Yb	0.119	0.189					0.13	0.186		0.278	0.284	0.265	0.302	0.212	0.275	0.21		0.16	0.16				0.202		
Lu	0.021	0.036					0.03	0.035		0.045	0.046	0.045	0.051	0.04	0.046	0.03		0	0.03				0.02		

DOI: 10.1344/105.000001715

TABLE II | **Major and trace element data, Bermeja Amphibolite, Puerto Rico**

Sample	AMPH-30	AMPH 31-93	AMPH 87-93	AMPH-101	AMPH-102	AMPH-105	AMPH 106-93	AMPH 108-93	AMPH 121-93	AMPH 125-93	AMPH-126-93	AMPH 127-93	AMPH-135-93	AMPH 136-93	LMG-84	LMG-89
SiO_2	48.79	45.95	45.28	-	50.91	53.36	43.77	40.95	44.35	50.72	51.76	50.74	47.42	50.70	-	-
TiO_2	0.71	0.96	1.18	-	1.53	1.05	1.16	0.88	1.17	1.83	0.88	1.05	2.14	0.99	-	-
Al_2O_3	12.09	12.53	13.24	-	13.17	15.13	13.86	14.47	12.86	13.33	15.54	15.46	14.65	14.54	-	-
Fe_2O_3	9.64	10.13	9.92	-	12.05	10.51	9.06	8.96	9.55	12.96	9.43	9.35	14.58	9.83	-	-
MnO	0.15	0.16	0.17	-	0.18	0.18	0.18	0.18	0.22	0.22	0.17	0.16	0.22	0.17	-	-
MgO	17.04	9.65	7.66	-	12.10	6.90	8.38	13.19	9.71	6.69	8.00	7.27	7.77	7.85	-	-
CaO	9.40	15.74	18.29	-	6.60	8.65	18.20	15.01	17.20	9.57	10.90	10.35	9.66	9.64	-	-
Na_2O	1.46	0.92	0.76	-	3.26	3.84	0.41	0.35	0.38	2.85	2.86	3.10	2.95	3.70	-	-
K_2O	0.05	0.06	0.07	-	0.41	0.27	0.07	0.03	0.09	0.13	0.47	0.65	0.51	0.26	-	-
P_2O_5	0.05	0.09	0.11	-	0.14	0.09	0.12	0.10	0.13	0.17	0.07	0.07	0.19	0.11	-	-
LOI	0.05	3.60	3.00	-	0.05	0.01	4.80	5.80	4.40	1.30	0.03	1.60	0.01	2.10	-	-
Subtotal	99.43	99.79	99.68	-	100.40	99.99	100.01	99.92	100.06	99.77	100.11	99.80	100.10	99.89	-	-
Cr	801	-	-	-	504	182	-	-	-	-	178	0	162	-	-	-
Ni	700.7304	178.1	297.2	-	457.573	64.7105	21	84.3	32.8	19.8	76.3691	25.8	83.6756	39.6	-	-
Co	0	56.7	57.3	-	-	-	42.3	47.7	59.6	60.6	-	52.9	0	57.7	-	-
Sc	39	35	42	40.1	31	30	34	35	35	42	31	37	59	39	34.1	42.2
V	216	266	288	-	324	271	253	270	266	396	254	295	4.07	263	-	-
Cu	61.0	28.3	50.7	-	45.8	5.2	58.3	85.3	19.5	58.0	34.6	75.5	22.4	25.2	-	-
Pb	2.0	0.8	0.3	-	-0.5	-0.4	1.2	1.1	1.4	0.4	1.7	0.4	3.8	0.4	-	-
Zn	41.9	18.0	20.0	-	66.5	82.4	14.0	31.0	21.0	26.0	46.0	13.0	105.0	31.0	-	-
W	0.0	107.1	139.7	-	-	-	73.7	48.8	165.7	153.6	-	119.4	-	110.8	-	-
Mo	0	0.1	0.1	-	-	-	0.1	0.1	0.2	0.1	-	0.1	-	0.1	-	-
Rb	0.18	0.70	2.00	-	1.94	3.22	0.90	1.20	1.30	2.10	7.02	10.70	6.64	4.80	-	-
Cs	-	0.1	0.2	0.2	-	-	-	0.3	-	0.1	-	0.4	-	0.1	0.25	0.25
Ba	115.8	77.0	14.0	-	107.8	55.6	167.0	177.0	68.0	27.0	128.9	711.0	53.0	60.0	-	-
Sr	296.2	246.7	347.9	-	141.0	176.3	40.7	43.0	36.7	182.6	511.5	445.6	143.0	148.9	-	-
Ga	11.9	13.9	14.1	-	15.7	14.1	16.2	14.3	16.0	19.5	11.8	16.8	18.7	18.6	-	-
Ta	-	0.3	0.3	-	-	-	0.2	0.2	0.5	0.6	-	0.4	-	0.4	-	-
Nb	0.4	1.9	2.4	1.1	1.9	2.2	1.4	1.1	1.8	3.2	0.9	2.0	5.9	2.2	1.7	1.4
Hf	1.1	1.2	0.9	1.8	2.5	2.0	2.0	0.9	2.2	3.1	1.5	2.3	3.4	1.9	2.3	2.5
Zr	29.4	45.0	22.9	55.0	95.0	66.3	65.1	22.1	68.0	99.0	49.5	63.9	129.7	53.9	74.0	75.0
Ti	4256.5	5755.0	7074.0	-	9172.0	6295.0	6954.0	0.0	7014.0	0.0	5276.0	6295.0	12829.0	5935.0	0.0	0.0
Y	14.6	23.7	23.2	19.0	30.2	20.9	27.0	19.8	29.2	45.2	18.8	25.4	44.2	27.0	23.9	25.8
Th	0.0	-	0.2	0.1	0.2	0.1	0.1	-	0.1	-	0.1	0.2	0.3	0.4	0.1	0.1
U	-0.6	-	-	0.1	1.9	0.0	-	-	-	-	-2.5	0.1	3.2	-	0.2	0.2
La	1.09	2.50	2.00	2.80	3.11	2.39	3.10	2.10	3.20	4.70	2.00	3.25	5.00	3.00	3.57	3.59
Ce	3.88	10.00	6.10	8.49	9.76	7.24	9.80	7.40	11.10	13.90	6.15	9.85	15.44	8.80	10.47	10.22
Pr	0.68	1.22	0.97	-	1.68	1.13	1.50	0.95	1.68	2.26	1.02	1.32	2.58	1.21	-	-
Nd	3.53	7.20	6.40	7.35	9.03	6.06	9.90	5.50	9.20	13.20	5.52	7.62	13.73	8.70	8.15	8.32
Sm	1.60	2.10	2.30	2.47	3.25	2.07	2.70	2.00	2.90	4.50	2.03	2.61	4.97	2.50	2.96	3.24
Eu	0.58	0.84	1.02	0.86	1.14	0.66	1.20	0.72	1.10	1.63	0.79	0.91	1.82	0.84	1.15	1.01
Gd	2.08	3.03	3.47	-	4.31	2.90	3.81	2.28	3.99	6.69	2.71	3.19	6.76	3.58	-	-
Tb	0.33	0.58	0.58	0.50	0.72	0.50	0.74	0.50	0.80	1.10	0.46	0.62	1.06	0.63	0.64	0.73
Dy	2.54	3.57	4.15	-	5.43	3.72	4.49	3.10	4.99	7.18	3.33	4.02	8.01	4.09	0.00	0.00
Ho	0.53	0.82	0.80	-	1.13	0.80	0.93	0.67	0.95	1.52	0.72	0.84	1.66	0.85	0.00	0.00
Er	1.57	2.42	2.48	-	3.37	2.40	2.81	2.02	2.89	4.48	2.11	2.68	4.86	2.70	0.00	0.00
Tm	0.24	0.38	0.37	-	0.48	0.35	0.41	0.29	0.43	0.73	0.31	0.41	0.70	0.44	0.00	0.00
Yb	1.55	2.43	2.27	2.06	3.14	2.38	2.69	2.01	2.77	4.95	2.07	2.50	4.50	2.90	2.59	2.73
Lu	0.24	0.35	0.36	0.30	0.48	0.36	0.38	0.31	0.39	0.70	0.31	0.42	0.72	0.47	0.35	0.35

DOI: 10.1344/105.000001715

TABLE III | **Major and trace element data, Lower Cajul Formation, Puerto Rico**

Sample Number	CAJ D	CAJ E	CAJ A	CAJ B	CAJ C	CAJDS 103B	LCAJ Z	LCAJ Y	LCAJ X	LCAJ V	LCAJ U
SiO_2	49.65	68.98	66.16	68.50	54.19	51.45	46.29	53.00	53.48	45.21	69.45
TiO_2	1.89	1.50	1.44	1.57	1.79	1.05	1.22	1.46	1.71	1.26	1.60
Al_2O_3	13.55	9.63	10.62	10.00	11.92	15.09	12.88	13.52	10.85	12.82	9.46
Fe_2O_3	12.38	6.71	9.18	8.22	13.57	9.96	9.11	11.02	12.78	9.26	7.35
MnO	0.21	0.07	0.10	0.08	0.15	0.19	0.18	0.17	0.15	0.18	0.08
MgO	6.99	1.80	2.13	1.58	4.81	7.70	10.24	6.63	4.91	11.82	1.61
CaO	8.78	4.98	4.88	4.81	6.44	10.03	15.48	8.22	9.75	14.21	5.26
Na_2O	2.99	3.56	3.48	3.77	4.06	3.09	0.45	3.64	2.26	0.37	3.06
K_2O	0.71	0.24	0.18	0.28	0.56	0.77	0.10	0.47	0.07	0.09	0.13
P_2O_5	0.15	0.35	0.32	0.38	0.17	0.08	0.12	0.15	0.17	0.13	0.36
LOI	2.60	2.10	1.40	0.70	2.20	0.03	3.90	1.60	3.80	4.60	1.60
SubTotal	99.90	99.92	99.89	99.89	99.86	99.44	99.97	99.88	99.93	99.95	99.96
Ni	34.6	10.9	11.2	16.3	24.8	50.3	28.5	33.3	22.9	42.7	11.3
Co	47.7	17.2	19.4	18.1	32.4	0	33.1	36.4	30.9	34.2	17.3
Sc	43	24	20	21	38	39	32	37	39	33	23
V	429	182	169	189	368	281	263	340	342	258	176
Cu	69.9	39.9	38.2	57.6	34.8	52.7	144.5	91.5	39.9	52.5	40
Pb	1.9	1.9	1	0.6	1.8	0.7	9.1	18.4	3.4	16.7	5.6
Zn	83	113	80	102	83	55	16	24	80	21	89
Rb	12.7	4.6	2	5.1	9.8	12.4	1	9	0	0.8	1.9
Cs	0.1	0.1	0	0.1	0	0	0	0.3	0	0	0
Ba	399	64	324	42	71	217	48	576.2	185.2	26	25.1
Sr	169.5	56.4	102.7	73.6	96	256.7	24.7	164.8	30.1	26.8	42.1
Ga	18.8	15.8	20	19.2	16.8	14.6	13.9	17.7	17.9	14.1	16.8
Ta	0.3	0.8	0.6	0.7	0.3	0	0	0.1	0.1	0.1	0.5
Nb	3.6	8.8	9.3	9.2	3	1.5	1.8	1.3	2.1	1.4	7.6
Hf	3.3	8.3	10.3	9.7	4.8	1.9	1.9	2.5	2.6	2.1	8.2
Zr	101	290	355.5	355	129.1	64.7	67.9	80.9	86.9	74.1	269.1
Y	46.2	97.9	110.1	111.7	48.1	22.1	27.5	36	46.8	29.3	91.1
Th	0.5	1	1.1	2	0.2	0.2	0	0	0	0.3	1.1
U	1	0.8	0.1	0.4	0	0	0	0	0	0	0.4
La	4.30	13.60	16.10	15.30	5.40	2.62	3.30	3.20	3.40	3.40	11.90
Ce	12.40	41.20	44.00	44.40	16.00	7.83	9.20	10.40	11.40	10.50	35.30
Pr	2.11	6.44	7.18	7.34	2.51	1.31	1.60	1.78	1.95	1.73	5.81
Nd	12.20	36.70	38.00	36.00	14.70	7.19	8.80	10.80	11.50	9.90	32.80
Sm	4.30	10.30	11.70	12.70	4.70	2.65	2.60	3.10	3.70	2.90	9.80
Eu	1.66	2.58	2.63	2.91	1.38	0.91	1.10	1.30	1.33	1.41	2.36
Gd	5.99	14.02	14.35	15.85	6.13	3.24	3.90	4.63	5.63	4.13	12.91
Tb	1.13	2.59	2.67	2.92	1.27	0.54	0.70	0.87	0.93	0.78	2.31
Dy	7.29	15.78	17.55	18.82	8.24	4.12	4.38	5.80	6.70	4.64	14.84
Ho	1.76	3.44	3.74	3.77	1.83	0.85	0.92	1.24	1.49	0.92	3.10
Er	4.68	9.55	11.58	12.01	5.46	2.38	2.77	3.51	4.53	3.01	9.02
Tm	0.68	1.52	1.58	1.62	0.76	0.36	0.40	0.52	0.74	0.44	1.38
Yb	4.52	9.42	10.00	10.27	4.66	2.33	2.66	3.41	4.50	2.75	9.22
Lu	0.68	1.35	1.56	1.46	0.73	0.37	0.43	0.58	0.70	0.45	1.37

Geologica Acta, 9(3-4), 273-287 (2011)
DOI: 10.1344/105.000001715

TABLE IV | **Sr-, Nd-, and Pb-isotope data, Pre-Arc Complex, southwestern Puerto Rico**

Sample	Unit	Rb	Sr	Sm	Nd	Pb	$m^{87}Sr/^{86}Sr$	$i^{87}Sr/^{86}Sr$	$m^{143}Nd/^{144}Nd$	$i^{143}Nd/^{144}Nd$	eNd	$^{206}Pb/^{204}PB$	$^{207}Pb/^{204}PB$	$^{208}Pb/^{204}PB$	Δ207/204	Δ208/204	Age (Ma)
AMPH-30	Las Palmas	0.2	296	1.6	3.5	2.0	0.703360	0.703355	0.513173	0.512838	8.56	18.35	15.72	38.35	23.99	53.79	185
AMPH-102	Las Palmas	1.9	141	3.2	9.0		0.704373	0.704270	0.513182	0.512916	10.18						185
AMPH-105	Las Palmas	3.2	176	2.1	6.1		0.703848	0.703714	0.513094	0.512842	8.63						185
AMPH-126-93	Las Palmas	7.0	511				0.703926	0.703825	ND								185
AMPH-127-93	Las Palmas	6.6	143	5.0	13.7		0.704319	0.703979	0.513027	0.512760	7.02						185
LCAJA	Lower Cajul	2.0	103	11.7	38.0	1.0	0.704330	0.704187	0.513040	0.512815	8.09	19.55	15.57	38.86	-4.02	-70.30	185
LCAJB	Lower Cajul	5.1	74	12.7	36.0	0.6	0.704500	0.703993	0.513066	0.512808	7.96	19.39	15.57	38.72	-2.29	-34.95	185
LCAJC	Lower Cajul	9.8	96	4.7	14.7	1.8	0.705160	0.704380	0.513070	0.512836	8.51	18.95	15.55	38.48	0.48	-5.76	185
LCAJDS/103B	Lower Cajul	12.4	257	2.7	7.2	0.7	0.704486	0.704131	0.513043	0.512768	7.19	18.70	15.55	38.16	3.19	-7.53	185
LCAJE	Lower Cajul	4.6	56	10.3	36.7	1.9	0.704450	0.703845	0.513046	0.512841	8.60	19.97	15.56	39.01	-9.58	-76.07	185

TABLE V | **Major and trace element data, Upper Cajul Formation, Puerto Rico**

Sample	UCAJN 103EXC	UCAJ-103EX-B	UCAJ-103EX-A	UCAJ-7-94NQ	UCAJ103EXF	UCAJ-103EX-D	UCAJ-106-93	UCAJ-103EX-E	UCAJ-103EX-G	UCAJ303/9.0A	UCAJ301/303A	UCAJNCOD	UCAJ99-93	UCAJ 303S/2	UCAJ 303S/3	UCAJ 303S/7	UCAJ 303S/1	UCAJS303S/2	UCAJS303S/4	UCAJ 303S/4	UCAJS303S/5
Facies	North	North	North	North	North	North	North	North	North	North	North	North	North	South	South	South	South	South	South	South	South
SiO_2	45.16	46.39	46.99	47.48	48.70	48.75	49.16	49.30	49.79	49.95	50.82	51.24	53.71	41.51	42.59	44.71	48.07	48.52	53.40	56.21	56.86
TiO_2	1.58	1.51	1.58	1.56	1.81	2.10	1.69	1.52	1.51	2.14	1.84	1.87	2.02	3.24	3.70	3.35	3.60	4.14	4.10	2.99	3.03
Al_2O_3	15.81	13.57	14.71	14.65	15.99	15.77	15.95	15.90	15.74	17.62	16.60	17.05	13.96	11.47	13.00	11.40	12.47	14.55	13.85	15.26	14.44
Fe_2O_3	9.44	11.97	8.89	11.09	10.47	12.28	8.56	8.80	10.21	11.59	10.74	10.34	11.31	9.63	10.48	10.12	9.93	9.63	9.70	9.70	9.81
MnO	0.03	0.16	0.12	0.16	0.10	0.16	0.10	0.19	0.20	0.15	0.16	0.15	0.09	0.13	0.08	0.10	0.08	0.09	0.09	0.10	0.10
MgO	4.67	5.45	5.36	4.91	3.68	3.75	3.82	4.84	4.65	2.85	3.91	3.61	4.51	2.44	2.18	3.43	2.56	2.44	2.83	1.45	1.47
CaO	9.50	9.27	9.96	8.80	6.63	7.37	7.33	9.00	7.14	5.99	5.13	4.63	5.24	15.48	13.19	13.45	9.93	8.45	6.23	3.34	3.38
Na_2O	3.72	3.45	3.52	4.29	2.94	3.95	3.16	3.79	4.56	3.63	5.27	5.31	4.05	3.32	4.11	3.49	3.95	4.60	4.39	7.06	7.14
K_2O	1.24	1.02	1.26	0.86	1.83	1.20	1.43	1.00	0.90	1.51	1.29	1.28	0.78	0.70	1.02	0.81	0.91	1.14	1.01	0.75	0.76
P_2O_5	0.19	0.19	0.19	0.19	0.24	0.25	0.21	0.17	0.18	0.38	0.24	0.25	0.20	0.55	0.70	0.63	0.70	0.78	0.78	0.70	0.70
LOI	7.50	6.50	6.50	5.40	6.80	4.40	7.70	5.00	4.30	4.10	3.80	4.00	3.10	11.20	8.60	8.40	7.50	4.60	3.50	2.30	2.30
SubTotal	98.84	99.48	99.08	99.39	99.19	99.98	99.11	99.51	99.18	99.91	99.80	99.73	98.97	99.67	99.65	99.89	99.70	98.94	99.88	99.86	99.99
Cr	165	0	0	0	172	0	0	0	0	129	41	48	82	0	0	0	0	7	41	0	7
Ni	45	43.2	63.5	26	49	26.9	57	71.7	42.8	43	49	59	37	86.8	100.4	23.3	79.2	118	91	74	77
Co	42	53.6	41.3	35.9	31	41.5	37.4	46	36.5	37	36	40	44	47.7	57.6	35.2	52.2	68	60	42.9	44
Sc	52	44	48	38	54	47	52	52	52	52	52	52	45	24	27	23	26	32	30	20	21
V	255	374	316	294	195	276	259	223	245	245	225	200	326	270	330	294	317	387	365	214	222
Cu	58	51.6	46.6	56.5	45	43.6	37.4	69	52.1	52	65	45	86	66.8	74	33.1	74.1	87	85	25.5	26
Pb	2	3.4	2.3	2.2	3	2.1	3.3	1.7	9.9	10	7	7	2	11.4	7.4	6.9	4.8	9	6	4.5	5
Zn	85	97	75	73	92	105	88	76	81	81	79	80	119	101	105	91	110	123	127	114	118
K	10294	8467	10460	7139	15191	9962	11871	8301	7471	12535	10709	9999	6475	5811	8467	6724	7554	9937	8695	6226	6446
Rb	32	25.3	28.9	16.7	40	32.6	32.7	22.4	27.7	28	27	30	14	5.6	7.9	14.2	7.7	9	9	18.1	17
Cs	0.9	1.3	0.9	1.2	1.9	1	1	0.7	1	1	0.5	0.7	0.4	0	0	0	0	0	0	0	0
Ba	163	175	170	442	160	163	176	146	187	187	120	139	225	596.2	264.3	218.1	345	310	397	153	158
Sr	246	221.8	246	507.2	193	286.3	219.3	249.2	377.3	377	281	309	267	276.8	263.1	257	249.4	309	287	471.7	488
Ga	18	16.4	18.3	18.5	16	19.2	18.2	14.2	16.8	17	16	19	16	17.7	18.1	20.5	19.3	21	22	15.3	16
Ta	0.5	0.5	0.6	0.5	0.6	0.7	0.6	0.5	0.6	0.6	0.7	0.7	0.8	2.4	2.6	2.5	2.6	3.05	2.99	3	3.11
Nb	8	8.7	10.2	9.5	9.3	11.5	10.2	7.1	8.3	8.3	8.8	9.3	10.9	39.5	41.6	36.5	42.5	48.8	48.9	46.4	48
Hf	2.4	2.9	2.8	2.6	2.5	3.1	3.2	2.2	2.2	2.2	3	3.3	3.5	7.8	8	7.6	8.1	9.39	9.32	6.1	6.32
Zr	88	94.9	100.9	93.3	99	125.9	102.5	79.6	88.7	89	101	106	118	268.7	293.2	264.5	290.3	344	334	233.3	242
Ti	9472	9052	9472	9352	10851	12589	10132	9112	9052	9052	11031	11211	12110	19424	22182	20083	21582	26032	24843	17925	18558
Y	30	31.6	31.7	27.2	39	42.8	38.3	27.7	30.6	31	39	42	36	34.1	44.1	37.4	40.5	52	47	33.8	35
Th	0.8	0.9	0.3	1.1	0.8	1.1	1.4	1	0.5	0.5	0.8	0.9	0.8	2.8	3.2	2.4	3.5	3.76	4.03	4.4	4.56
U	0.3	0.4	0.7	0.3	0.3	0.4	0.3	0.5	0.3	0.3	0.4	0.4	0.7	4.6	3.6	1.9	4.6	4.22	5.29	0.8	0.83
La	6.9	8.1	8.3	9	9.3	12.2	9.1	6.6	7.5	7.5	9.5	10.4	9.9	30	34.9	30.6	32.9	40.96	37.87	38.3	39.65
Ce	16.4	18.3	19.3	20.8	21.9	25.1	21.7	16	18.2	18.2	22.4	25	22.3	67.5	78	67.8	74.7	91.54	85.99	78	80.76
Pr	2.48	2.52	2.8	2.88	3.12	3.73	3.11	2.24	2.47	2.47	3.08	3.52	3.44	8.28	9.75	9.06	9.51	11.44	10.95	9.33	9.66
Nd	13.6	14.7	14.4	14.7	16.3	19.4	17.3	12	14.8	14.8	15.8	16.6	19.1	35.3	43.7	42.2	42.7	51.29	49.15	42.8	44.31
Sm	3.4	3.7	4.3	3.9	4.4	5.1	4.7	3.1	3.5	3.5	4.3	4.7	4.2	8.1	9.5	8.4	9	11.15	10.36	7.8	8.08
Eu	1.28	1.48	1.44	1.27	1.39	1.83	1.81	1.17	1.39	1.39	1.65	1.78	1.7	2.67	3.27	2.82	3.13	3.84	3.6	2.83	2.93
Gd	4.95	5.43	5.7	5.55	6.36	6.7	6.31	4.47	4.44	4.44	5.72	6.5	6.57	8.55	9.91	8.52	9.61	11.63	11.06	7.6	7.87
Tb	0.81	0.86	0.87	0.81	1.07	1.17	1.06	0.73	0.8	0.8	1	1.12	1.07	1.37	1.63	1.31	1.54	1.91	1.77	1.14	1.18
Dy	5.52	5.28	5.03	5.13	5.69	7	6.66	4.07	5.27	5.27	6.15	6.85	5.8	6.56	7.31	7.2	7.74	8.58	8.91	6.54	6.77
Ho	1.07	1.12	1.14	0.92	1.3	1.43	1.35	0.96	1.08	1.08	1.28	1.43	1.27	1.18	1.4	1.27	1.4	1.64	1.61	1.13	1.17
Er	3.06	3.22	3.52	2.66	3.88	4.01	3.65	2.86	2.87	2.87	3.69	4.05	3.77	3.43	4.08	3.31	3.93	4.79	4.52	3.15	3.26
Tm	0.45	0.45	0.43	0.4	0.53	0.61	0.49	0.42	0.48	0.48	0.57	0.63	0.51	0.43	0.48	0.51	0.51	0.56	0.59	0.45	0.47
Yb	2.5	3.02	2.81	2.65	2.94	3.76	2.71	2.29	2.76	2.76	3.4	3.75	3.37	2.56	3.14	2.83	3.07	3.69	3.53	2.59	2.68
Lu	0.36	0.44	0.48	0.38	0.48	0.61	0.42	0.36	0.39	0.39	0.5	0.57	0.5	0.4	0.48	0.44	0.43	0.56	0.49	0.43	0.45

TABLE VI | **Sr-, Nd- and Pb-isotope data, Upper Cajul Formation, southwestern Puerto Rico**

Sample	Unit	Rb	Sr	Sm	Nd	Pb	$m^{87}Sr/^{86}Sr$	$i^{87}Sr/^{86}Sr$	$m^{143}Nd/^{144}Nd$	$i^{143}Nd/^{144}Nd$	eNd	$^{206}Pb/^{204}PB$	$^{207}Pb/^{204}PB$	$^{208}Pb/^{204}PB$	Δ207/204	Δ208/204	Age (Ma)
UCAJN103C	Upper Cajul	32.0	246	3.4	13.6	2.0	0.705220	0.704780	0.512925	0.512841	6.09	18.85	15.65	38.50	11.57	8.34	85
UCAJN103D	Upper Cajul	33.0	286	5.1	19.4	2.1	0.704910	0.704520	0.512921	0.512833	5.93	19.24	15.57	39.05	-0.66	16.18	85
UCAJN103G	Upper Cajul	27.7	377	3.5	14.8	9.9	0.704950	0.704702	0.513047	0.512967	8.56	19.25	15.59	38.90	1.23	-0.03	85
UCAJN103A	Upper Cajul	28.9	246	4.3	14.4	2.3	0.705010	0.704613	0.512985	0.512885	6.95	19.29	15.60	39.18	1.80	23.14	85
UCAJS303/S3	Upper Cajul	7.9	263	9.5	43.7	7.4	0.704640	0.704539	0.512823	0.512750	4.32	21.15	15.65	40.43	-13.37	-76.74	85
UCAJS303/S5	Upper Cajul	17.0	488	8.1	44.3	5.0	0.703980	0.703862	0.512848	0.512787	5.03	21.01	15.67	40.51	-9.85	-51.81	85

TABLE VII | **Major and trace element data, Caribbean Cretaceous Basalt Plateau**

Sample	CCBP-146-43E	CCBP-150-12R	CCBP-151-14R	P-152=24-CC-R	CCBP-153-20R	CBP151-13-CC	CBP146-42R-1	OIB	NMORB	E-MORB
SiO_2	48.42	46.60	48.69	48.65	49.29	46.78	46.88	-	-	-
TiO_2	1.08	1.23	3.33	1.69	1.79	2.74	0.97	-	-	-
Al_2O_3	14.77	14.07	12.60	11.69	13.71	14.28	13.72	-	-	-
Fe_2O_3	11.36	11.43	13.19	15.26	13.48	12.72	10.92	-	-	-
MnO	0.16	0.21	0.12	0.12	0.28	0.09	0.20	-	-	-
MgO	10.37	9.00	9.10	9.36	10.32	5.69	7.80	-	-	-
CaO	11.88	12.95	8.01	8.70	9.50	8.84	13.33	-	-	-
Na_2O	2.10	2.13	2.56	2.28	2.52	2.36	1.77	-	-	-
K_2O	0.08	0.09	0.92	1.05	0.10	1.15	0.30	-	-	-
P_2O_5	0.10	0.10	0.26	0.17	0.12	0.31	0.11	-	-	-
LOI	-	-	-	-	-	4.60	3.50	-	-	-
Subtotal	100.32	97.81	98.78	98.97	101.11	99.56	99.50	-	-	-
Cr	363	329	410	251	149	0.043	0.045	-	-	-
Ni	121	115	132	56	90	133	156	-	-	-
Co	-	-	-	-	-	49.7	75.5	-	-	-
Sc	44	45	43	53	60	39	45	-	-	-
V	296	315	491	459	506	406	296	-	-	-
Cu	125	143	222	44	192	-	-	-	-	-
Pb	0.4	0.3	2.78	0.78	18.31	0.8	0.1	-	-	-
Zn	54	58	132	115	106	-	-	-	-	-
Rb	1.3	0.69	14.7	24.2	1.9	38.1	5.3	-	-	-
Cs	0.03	0	0.13	0.37	0.01	0.7	-	-	-	-
Ba	12.16	10.85	80	7.18	20.35	51	13	-	-	-
Sr	125.6	113.6	332.5	96.3	161.5	301.3	125	-	64	6.4
Ga	14	16	25	17	19	22.1	16.1	-	-	-
Ta	0.58	0.49	1.64	0.41	0.56	1.5	0.6	2.7	0.132	0.47
Nb	3.4	4.4	26.4	2.5	6.1	20.2	3	48	2.33	8.3
Hf	1.43	1.67	4.82	2.19	2.445	4.1	1.4	7.8	2.05	2.03
Zr	53.7	59.5	188.6	77.4	89.4	150	45.8	280	74	73
Ti	6474.6	7373.85	19963.35	10131.55	10731.05	-	-	17200	7600	6000
Y	18.6	22.6	28.8	33.22	24.01	30.9	21.8	29	28	22
Th	0.19	0.231	1.616	0.12	0.4	1.7	0.2	4	0.12	0.6
U	0.045	0.32	1.21	0.315	0.18	1.9	0.2	1.02	0.047	0.18
La	2.45	2.99	15.83	2.17	4.12	16.4	2.9	37	2.5	6.3
Ce	6.85	7.97	38.83	6.52	11.21	36.7	6.7	80	7.5	15
Pr	1.09	1.38	5.58	1.24	1.76	4.91	1.11	9.7	1.32	2.05
Nd	5.82	6.8	25.89	7.5	9.24	25.5	5.9	38.5	7.3	9
Sm	2.15	2.41	6.52	3.07	3.12	6.7	2.3	10	2.63	2.6
Eu	0.8	0.86	2.29	1.1	1.2	2.17	0.83	3	1.02	0.91
Gd	2.67	3.33	7	4.54	4.1	6.23	2.95	7.62	3.68	2.97
Tb	0.52	0.6	1	0.83	0.65	0.96	0.55	1.05	0.67	0.53
Dy	3.328	4.06	6.145	5.87	4.54	5.54	3.63	5.6	4.55	3.55
Ho	0.72	0.86	1.15	1.27	0.97	1.16	0.82	1.06	1.01	0.79
Er	2.04	2.43	2.98	3.81	2.74	2.8	2.29	2.62	2.97	2.31
Tm	0.31	0.34	0.41	0.55	0.42	0.4	0.4	0.35	0.456	0.356
Yb	1.94	2.41	2.29	3.6	3.08	2.37	2.14	2.16	3.05	2.37
Lu	0.31	0.37	0.33	0.53	0.49	0.34	0.39	0.3	0.455	0.345

TABLE VIII | **Major and trace element data, Atlantic and Caribbean Pelagic Sediments**

Sample	Unit	SiO_2	TiO_2	Al_2O_3	Fe_2O_3	MnO	MgO	CaO	Na_2O	K_2O	P_2O_5	LOI	SubTotal	Cr	Ni
105/15/6	AKPS	54.78	0.64	14.60	5.92	0.02	2.30	0.48	1.88	3.00	0.05	16.00	99.67	0.007	154
105/18/6	AKPS	14.63	0.14	3.20	1.89	0.05	0.83	40.28	0.74	0.88	0.03	36.80	99.47	0.002	47
105/37/5	AKPS	47.04	0.42	9.59	5.13	0.19	1.90	14.40	0.93	2.17	0.07	18.00	99.84	0.004	94
105/37/6	AKPS	44.43	0.53	10.63	6.18	0.58	2.35	13.62	0.94	2.80	0.05	17.50	99.61	0.007	113
417D/17/3	AKPS	55.53	0.41	9.11	3.93	0.03	3.37	2.85	1.11	2.17	1.58	19.60	99.69	0.017	122
417D/18/2	AKPS	56.78	0.51	11.85	5.46	0.05	4.89	0.50	1.45	2.67	0.09	15.50	99.75	0.014	75
417D/19/1	AKPS	74.60	0.31	7.06	4.00	0.02	1.76	0.62	0.81	1.91	0.26	8.30	99.65	0.008	61
417D/21/3	AKPS	25.62	0.24	4.78	15.18	0.06	1.53	7.85	0.74	1.90	0.46	32.50	90.86	0.006	192
CKPS 4	CKPS	35.76	0.39	8.40	5.71	0.20	2.76	24.39	1.43	1.82	0.17	18.60	99.63	-	101.6
CKPS 5	CKPS	55.04	0.38	9.68	4.82	0.15	1.97	12.30	2.63	1.81	0.15	10.60	99.53	-	39.5
CKPS 6	CKPS	58.71	0.59	13.94	8.42	0.22	2.18	3.42	2.43	2.54	0.20	7.30	99.95	-	35
CKPS 7	CKPS	45.25	0.21	5.16	2.47	0.17	1.03	24.41	0.88	0.92	0.12	19.20	99.82	-	23.1
CKPS 9ABLU	CKPS	63.05	0.64	15.33	3.58	0.11	1.21	1.22	5.15	3.88	0.15	5.20	99.52	-	2.4
CKPS 9AGRN	CKPS	64.51	0.67	14.35	3.58	0.12	1.26	1.51	4.99	3.20	0.17	5.00	99.36	-	3.1
CKPS 9B	CKPS	58.06	0.59	14.29	3.04	0.07	1.63	5.33	1.17	2.28	0.16	12.70	99.32	-	2.7
CKPS 9C	CKPS	59.65	0.68	14.74	6.24	0.19	2.48	5.01	4.59	2.26	0.28	3.70	99.82	-	22
MQT-1	PJKC	95.19	0.01	0.25	0.01	-	0.03	0.02	-	0.03	-	-	95.54	26	-
MQT-64	PJKC	97.24	0.01	0.48	0.12	-	0.15	0.04	-	0.08	0.01	-	98.13	90	-
MQT-65-94PG	PJKC	96.60	0.02	0.61	0.39	0.01	0.07	0.15	0.05	0.07	0.02	0.50	98.49	-	1.8
MQT-66-94G	PJKC	96.09	0.04	0.92	0.79	0.01	0.10	0.12	0.12	0.07	0.03	0.90	99.19	-	6.1
MQT-88	PJKC	98.83	0.06	1.14	0.30	0.01	0.23	0.13	0.32	0.16	0.02	0.00	101.20	96	21
MQT-94-94DG	PJKC	96.57	0.04	0.71	0.49	0.01	0.09	0.12	0.11	0.07	0.03	0.70	98.94	-	4.2
MQT-96A-94RR	PJKC	86.40	0.02	0.24	11.63	0.02	0.07	0.11	0.02	0.02	0.04	1.00	99.57	-	19
MQT-JUR	PJKC	100.24	0.01	0.33	0.07	-	0.16	0.05	0.02	0.04	-	-	100.92	33	-
oib	WIP	-	-	-	-	-	-	-	-	-	-	-	-	-	-
e-morb	WIP	-	-	-	-	-	-	-	-	-	-	-	-	-	-
n-morb	WIP	-	-	-	-	-	-	-	-	-	-	-	-	-	-

Sample	Co	Sc	V	Cu	Pb	K	Rb	Cs	Ba	Sr	Ga	Ta	Nb	Hf	Zr	Ti	Th	U
105/15/6	29	15	125	-	17.3	24904	125	7.1	524	184.7	18.3	0.8	12.7	3.2	101.4	3837	11.3	2.6
105/18/6	12.9	4	54	-	7.6	7305	38.4	1.9	1000	493.6	4.3	0.2	3.5	0.9	28	839	3.6	2.2
105/37/5	26.8	10	65	-	15.9	18014	91.3	4.4	176	141.5	13	0.6	8.3	2.2	74.5	2518	6	0.7
105/37/6	47.2	12	89	-	17.8	23244	108.4	6	243	146.6	15	0.7	10.6	3.5	105.6	3177	7.7	0.9
417D/17/3	16.4	11	283	-	13	18014	90.8	5.1	1000	139.8	12.7	0.5	7.2	1.9	74.4	2458	6.4	9.6
417D/18/2	15.6	14	92	-	12.6	22164	124.3	6	635	67.5	19.8	0.7	9.4	2.6	95.9	3057	7	2.2
417D/19/1	12	10	81	-	15.6	15855	83.6	4.7	1948	95.5	7.8	0.3	4	1.4	54.3	1858	7.4	0.6
417D/21/3	10.5	5	480	-	13.4	15772	72.4	3	1015	134.6	7.6	0.3	4.4	1.3	48.7	1439	3.8	7.1
CKPS 4	23	15	149	77.3	26.1	15108	71.9	0.7	954	401.4	13.1	0.097	1.4	1.1	32.9	2338	1.2	0.9
CKPS 5	16.7	12	116	65.1	12.2	15025	49.9	0.3	1962	583.9	11.8	0.18	2.8	1.3	43.6	2278	1.6	0.8
CKPS 6	23.1	16	189	127.6	10.1	21085	99.8	1.2	1383	369	20.6	0.16	2.6	1.7	46.5	3537	1.2	0.5
CKPS 7	9.7	4	52	42.3	21.6	7637	26.3	1.5	1933	535.9	6.5	0.1	1.7	1.2	36.3	1259	1.8	0.6
CKPS 9ABLU	1.5	6	37	11.2	11.7	-	88.3	4.8	887	153.6	17.9	0.4	7.6	3.8	153.6	-	7.1	1.7
CKPS 9AGRN	4.3	7	36	12.9	11.4	-	61.3	4.2	839	169.8	13.3	0.4	7	3.8	148.2	-	6	2.2
CKPS 9B	2.1	6	32	11.8	15.1	18927	94.1	1.2	3235	3234	16.9	0.4	7.2	4.3	145.3	3537	7.9	2.6
CKPS 9C	16	18	122	43.6	47.7	18761	34.1	-	923	190	16.4	0.3	4.1	2.7	93.8	4077	4.3	1.4
MQT-1	-	-	-	-	0.82	249	0.94	0.14	1726	141.1	-	0.1	1.7	0.07	4.95	60	0.11	0.24
MQT-64	-	-	6	-	0.87	664	2.08	0.09	390	12.99	3	0.08	1.4	0.09	9.1	60	0.14	0.1
MQT-65-94PG	-	2	42	6.7	0.9	-	1.7	-	6951	65.8	1.1	0.2	1	-	10	-	0.2	0.2
MQT-66-94G	1.4	1	12	31.1	3.4	-	2.6	-	1400	36.2	1.5	-	0.7	-	14.4	-	0.2	0.4
MQT-88	-	-	23	110	3.37	1328	4.55	0.13	768	24.19	-	0.14	2.5	0.24	26.6	360	0.58	0.37
MQT-94-94DG	2.9	2	25	27.5	2.6	-	2	-	1178	28.7	2.3	-	1.6	-	16.6	-	0.3	1
MQT-96A-94RR	2.7	-	23	16.9	1.6	-	-	-	2671	16.4	0.9	-	0.6	-	3.6	-	0.3	0.1
MQT-JUR	-	-	24	-	3.34	332	1	0.09	717	15.7	-	0.07	1.3	0.06	5.6	60	0.06	0.11
oib	-	-	-	-	3.2	12000	21	0.387	350	660	-	2.7	48	7.8	280	17200	4	1.02
e-morb	-	-	-	-	0.6	2100	5.04	0.063	57	155	-	0.47	8.3	2.03	73	6000	0.6	0.18
n-morb	-	-	-	-	0.33	600	0.56	0.007	6.3	510	-	0.132	2.33	2.05	74	7600	0.12	0.047

TABLE VIII | **Continued**

Sample	La	Ce	Pr	Nd	Sm	Eu	Gd	Tb	Dy	Ho	Er	Tm	Yb	Lu
105/15/6	34	69.3	6.81	27.7	6.2	1.04	4.51	0.69	4.04	0.81	2.26	0.32	2.47	0.37
105/18/6	18	28.6	3.61	14.9	3.6	0.68	3.13	0.42	2.47	0.5	1.29	0.18	1.03	0.18
105/37/5	32.1	62.6	6.66	26.6	5	1.19	4.38	0.65	3.88	0.72	2.04	0.31	1.82	0.28
105/37/6	37.6	69.9	7.51	31.8	6.4	1.14	5.13	0.7	4.04	0.88	2.53	0.38	2.43	0.37
417D/17/3	42.6	58.8	8.49	38	7.7	1.64	7.57	1.1	6.54	1.53	4.19	0.63	4.11	0.61
417D/18/2	23.8	46.3	5.26	20.3	4.2	0.79	3.25	0.53	2.81	0.57	1.79	0.31	1.94	0.31
417D/19/1	42.9	83.1	11.86	54.3	9.1	2.46	9.95	1.65	8.77	1.71	4.34	0.61	3.88	0.54
417D/21/3	37.7	71.5	9.34	39.5	9	1.93	8.22	1.23	6.71	1.3	3.55	0.49	2.88	0.47
CKPS 4	9.3	13.1	2.03	9.2	2	0.62	2.24	0.39	2.31	0.47	1.4	0.23	1.55	0.21
CKPS 5	11.9	23.5	2.74	14.2	2.9	0.64	2.83	0.46	2.52	0.53	1.63	0.26	1.63	0.25
CKPS 6	16.8	21.8	3.65	19.8	3.6	1.08	3.81	0.6	3.9	0.74	2.06	0.31	2.07	0.31
CKPS 7	15.5	16.9	3.04	14	2.4	0.64	2.69	0.39	2.47	0.49	1.59	0.25	1.5	0.21
CKPS 9ABLU	32	58.8	6.96	31.7	6.2	1.64	5.33	0.72	4.32	0.89	2.35	0.35	2.43	0.36
CKPS 9AGRN	36.5	65.5	7.68	36.2	6	1.58	5.45	0.8	4.92	1	2.73	0.44	2.65	0.49
CKPS 9B	34.3	64.3	7.68	33.2	6.4	1.53	5.61	0.89	5.46	1.01	3.2	0.51	3.76	0.48
CKPS 9C	18.6	33.8	4.35	21.6	4.6	1.27	4.35	0.66	3.78	0.82	2.44	0.36	2.48	0.37
MQT-1	0.47	0.54	0.09	0.44	0.14	0.078	0.08	0.01	0.08	0.01	0.05	0.005	0.05	0.009
MQT-64	1.09	1.62	0.29	1.41	0.3	0.09	0.34	0.05	0.27	0.05	0.15	0.02	0.13	0.03
MQT-65-94PG	1.3	2.2	0.36	1.6	0.5	-	0.46	0.1	0.35	0.06	0.13	-	0.17	0.01
MQT-66-94G	2.7	4.1	0.61	2.7	0.3	-	0.58	0.09	0.58	0.13	0.39	0.08	0.55	0.1
MQT-88	2.48	3.81	0.66	2.89	0.66	0.17	0.63	0.11	0.69	0.14	0.42	0.062	0.55	0.08
MQT-94-94DG	2.4	3.1	0.59	2.8	0.5	0.11	0.59	0.09	0.54	0.09	0.24	0.06	0.35	0.04
MQT-96A-94RR	2.8	2.6	0.51	2.5	0.2	0.08	0.68	0.09	0.62	0.12	0.25	-	0.25	0.03
MQT-JUR	0.88	1.44	0.22	0.79	0.2	0.08	0.15	0.03	0.12	0.04	0.07	0.02	0.13	0.02
oib	37	80	9.7	38.5	10	3	7.62	1.05	5.6	1.06	2.62	0.35	2.16	0.3
e-morb	6.3	15	2.05	9	2.6	0.91	2.97	0.53	3.55	0.79	2.31	0.356	2.37	0.354
n-morb	2.5	7.5	1.32	7.3	2.63	1.02	3.68	0.67	4.55	1.01	2.97	0.456	3.05	0.455

TABLE IX | **Sr-,Nd- and Pb-isotope data, Atlantic and Caribbean Pelagic Sediments**

Sample	Rb	Sr	Sm	Nd	Pb	$m^{87}Sr/^{86}Sr$	$i^{87}Sr/^{86}Sr$	$m^{143}Nd/^{144}Nd$	$i^{143}Nd/^{144}Nd$	eNd	$^{206}Pb/^{204}PB$	$^{207}Pb/^{204}PB$	$^{208}Pb/^{204}PB$	Δ207/204	Δ208/204	Age (my)
CKPS4	71.9	401.4	2.0	9.2	26.1	0.70577	0.70513	0.512726	0.512649	2.467	18.90	15.65	38.60	11.02	12.29	90
CKPS5	49.9	583.9	2.9	14.2	12.2	0.70592	0.70561	0.512727	0.512654	2.578	18.92	15.61	38.68	6.81	17.87	90
CKPS6	99.8	369.0	3.6	19.8	10.1	0.70583	0.70486	0.512659	0.512594	1.407	18.94	15.61	38.75	6.59	22.45	90
CKPS7	26.3	535.9	2.4	14.0	21.6	0.70598	0.70580	0.512512	0.512451	-1.389	18.87	15.65	38.63	11.35	18.92	90
CKPS9b	94.1	3234.4	6.4	33.2	15.1	0.70522	0.70512	0.512851	0.512782	5.077	19.11	15.62	38.89	5.75	15.90	90
CKPS9c	34.1	190.0	4.6	21.6	47.7	0.70478	0.70414	0.512921	0.512845	6.302	18.89	15.65	38.60	11.13	13.50	90
417D/12/3	90.8	139.8	7.7	38.0	16	0.71489	0.71243	0.512083	0.512007	-9.929						95
105/15/6	125.0	184.7	6.2	27.7	17	0.71436	0.71140	0.512119	0.512022	-9.266	18.88	15.69	38.93	15.24	47.71	110
417D/18/2	124.3	67.5	4.2	20.3	15	0.72837	0.72103	0.511963	0.511881	-12.256	18.99	15.68	39.06	13.05	47.41	100
105/18/6	38.4	493.6	3.6	14.9	12	0.70821	0.70785	0.512196	0.512086	-7.882	18.93	15.68	38.86	13.70	34.66	115
417D/19/1	83.6	95.5	11.1	54.3	17	0.71488	0.71122	0.512187	0.512102	-7.821	18.90	15.72	39.08	18.02	60.29	105
417D/21/3	72.4	134.6	9.0	39.5	24	0.71302	0.71067	0.512202	0.512103	-7.681	19.33	15.71	38.86	12.36	-13.70	110
105/37/5	91.3	141.5	5.0	26.6	20	0.71425	0.71065	0.512151	0.512047	-8.020	18.75	15.70	38.97	17.65	67.43	140
105/37/6	108.4	146.6	6.4	31.8	22	0.71661	0.71234	0.512135	0.512020	-8.428	18.73	15.69	38.92	16.87	64.84	145

DOI: 10.1344/105.000001715

TABLE X | **Major and trace element data, Early Island Arc, Western Puerto Rico**

Sample*	BQN 300-3.6D	BQN 103-9.8A	BQN 300-1.7A	BQN 300-8	BQN 103-9.8D	BQN 300-1.2D	BQN 118-93	BQN 300-1.7C	BQN 103-9.8B	BQN 103-9.8C	BQN 300-1.7B
SiO_2	50.33	52.05	52.63	52.72	53.69	53.99	54.06	54.28	54.53	62.40	63.63
TiO_2	0.72	0.75	0.84	1.01	0.80	0.75	0.75	0.81	0.82	1.02	0.80
Al_2O_3	14.21	16.27	17.48	15.80	17.33	14.67	15.34	17.39	16.86	17.11	15.35
Fe_2O_3	9.15	8.14	8.88	7.87	8.72	9.46	6.29	8.06	8.46	6.64	7.32
MnO	0.20	0.10	0.20	0.17	0.14	0.14	0.37	0.17	0.16	0.09	0.09
MgO	3.95	3.72	4.36	2.61	4.00	4.87	2.07	3.20	3.70	0.60	1.12
CaO	9.14	7.64	9.05	6.80	7.25	8.24	8.89	7.96	7.10	5.05	2.74
Na_2O	3.44	1.77	2.47	5.55	2.99	3.51	4.81	3.29	3.05	3.24	6.30
K_2O	0.61	0.29	0.79	0.61	1.86	2.21	0.42	1.67	2.11	2.09	0.50
P_2O_5	0.32	0.33	0.34	0.36	0.36	0.33	0.28	0.36	0.37	0.32	0.31
LOI	7.4	8.8	2.7	6.3	2.7	2.0	6.4	3.0	2.5	1.4	2.1
Total	99.47	99.86	99.74	99.80	99.84	100.17	99.68	100.19	99.66	99.96	100.26
Cr	369	21	22	7	22	335	103	28	27	28	21
Ni	112	8.4	8.9	6.2	14.9	32.9	42.7	13.9	12.6	6	6.5
Co	35.3	22.7	27.2	20.2	27.2	35.3	25.5	25.3	22.2	10.7	15.2
Sc	29	18	23	17	23	35	25	25	20	17	17
V	143	188	228	180	197	244	190	225	202	165	176
Cu	55.5	16.9	97.1	44.7	73.3	7.3	101.6	16.4	57.4	22.9	32.8
Pb	6.2	3.1	26.8	7.5	31.4	3	2.4	4.2	2.2	3.6	4.4
Zn	54	47	50	68	67	50	62	76	70	46	33
Rb	14.7	2.2	6.2	11.1	41.5	39.9	5.4	26.5	42.6	48.4	8.4
Cs	0.5	0.7	0	0.9	0.3	0.9	0.3	0.8	0.2	0.8	0.9
Ba	398	289	1046	444	865	1394	1427	1399	895	943	437
Sr	561.6	360.4	1384.6	474.1	581	651.7	572.9	752.6	566.4	525.4	505.3
Ga	17.3	19.9	19.2	16.1	19.9	16.2	15.7	20.4	20.3	18	12.9
Ta	0.8	0.9	0.8	1.7	1	0.8	0.9	1	0.8	1.8	1.6
Nb	10.9	11.8	11.6	24.9	13.4	10.6	11.8	13.3	13.4	26	23.5
Hf	3.8	3.5	3.6	4.5	3.4	3.3	3.7	3.9	3.6	4.9	4.8
Zr	121.8	136.1	111.6	184.3	125.4	114.7	124	129.5	147	181.2	160.2
Y	21.4	20.2	20.5	24	23.4	19.7	21.1	22.5	21.7	35.8	18.6
Th	3.2	3.5	3.9	3.8	4.4	4.4	3.3	4.7	3.7	5.9	5.3
U	0.4	1.1	1.7	1.3	1.6	0.8	1.1	1.4	1.5	1.8	1.5
La	22.7	20.7	22.2	33.5	23	18.5	23.1	22.6	21.9	35	34.6
Ce	43.5	40.2	40.8	60.1	43.9	36.7	40.6	41.8	43.1	60.8	56.4
Pr	5.34	4.83	5.23	7.24	5.76	4.79	5.3	5.59	5.29	7.68	6.57
Nd	21.8	19.6	23.1	26.9	23.6	21.2	21.3	23.5	21.3	30.4	25
Sm	4.3	3.7	4.3	6	4.7	4.1	4.2	4.7	4.2	5	4.9
Eu	1.19	1.46	1.19	1.67	1.36	1.09	1.26	1.33	1.38	1.78	1.33
Gd	3.71	3.63	4.16	4.4	4.22	4.38	4.46	4.47	4.08	4.76	3.86
Tb	0.61	0.62	0.61	0.68	0.65	0.6	0.63	0.66	0.59	0.82	0.55
Dy	3.35	4	3.54	3.96	3.99	3.49	3.63	3.59	3.99	5.04	3.44
Ho	0.66	0.72	0.67	0.69	0.72	0.74	0.69	0.85	0.73	1.14	0.66
Er	2	2.13	1.9	2.15	2	1.94	1.98	2.2	2.11	3.17	1.86
Tm	0.3	0.32	0.3	0.34	0.35	0.32	0.29	0.32	0.25	0.47	0.29
Yb	2.1	2.31	1.83	2.29	2.21	1.99	1.94	1.96	1.93	3.14	1.77
Lu	0.36	0.31	0.34	0.34	0.31	0.32	0.35	0.38	0.31	0.45	0.32

* Boquerón (BQN) & Río Loco (RL) data adapted from Jolly et al. (2007).

DOI: 10.1344/105.000001715

TABLE X | **Continued**

Sample*	LJS 07-02	LJS 100-9.3	LJS 300-5.1	LJS 103-5.7	LJS 103-12.3B	LJS 110-93	LJS 300-4.8	LJS 300-4.1	LJS 301-4.2	LJS 312-2.1A	RL371/4.1
SiO_2	55.42	55.75	55.97	56.79	56.98	57.17	58.30	62.11	62.22	63.88	51.74
TiO_2	0.83	1.17	0.71	0.82	0.85	0.88	0.81	0.75	0.91	0.83	0.75
Al_2O_3	16.32	17.13	16.19	16.46	17.53	16.09	17.60	16.64	15.30	16.03	10.84
Fe_2O_3	6.68	8.45	6.65	6.35	7.90	7.56	7.09	5.13	6.45	6.53	8.97
MnO	0.11	0.14	0.17	0.20	0.19	0.12	0.10	0.07	0.09	0.05	0.19
MgO	2.65	2.53	2.93	0.86	1.74	4.07	2.68	0.63	2.03	0.70	7.78
CaO	7.32	4.12	7.09	6.34	6.04	3.06	4.16	4.26	6.21	4.38	8.61
Na_2O	2.86	5.91	2.99	5.14	3.79	3.94	3.26	5.71	3.10	3.43	2.93
K_2O	0.34	0.78	1.61	1.67	1.22	2.39	2.70	1.09	1.50	2.34	1.65
P_2O_5	0.29	0.33	0.32	0.28	0.26	0.32	0.29	0.30	0.29	0.24	0.24
LOI	7.0	3.5	5.4	5.4	3.3	4.1	3.2	3.0	1.8	1.4	6.4
Total	99.82	99.81	100.03	100.31	99.80	99.70	100.19	99.69	99.90	99.81	100.10
Cr	-	-	-	-	-	-	-	-	-	-	422
Ni	2.8	9.4	4.2	11.3	6.5	6.7	6.1	3.9	52.7	14.4	60
Co	17.7	19.7	15.5	13	22.8	19.3	18.6	6.7	14.6	12.3	36
Sc	15	17	12	17	16	17	17	13	17	17	26
V	146	182	130	149	173	143	112	149	175	114	221
Cu	25.5	38.2	16.4	36.4	19.1	18.4	12	92.2	29.6	26.6	33
Pb	2.4	4	3.6	2.3	2.5	18.5	3.3	14	35.9	31.5	1
Zn	48	76	53	34	73	59	56	18	28	18	70
Rb	3.5	11.4	36	35.4	21.8	40.3	56.4	24.5	34.1	47.8	33
Cs	0.7	0.6	1	0.8	0.5	0.5	0.4	0.9	0.4	0.4	0.3
Ba	654	616	988	899	961	974	1191	678	1059	1515	1486
Sr	369.4	563.5	546.6	581.3	511.3	400.3	489.8	676.8	546.4	549.9	212
Ga	18.2	20	17.8	19.3	18.7	20.4	20.3	14.6	19.9	17.7	19
Ta	1.7	1.6	1.6	1.4	1.6	1.4	1.5	1.6	1.4	1.3	0.8
Nb	21	29.1	22.8	19	22.7	19	18.9	21.1	20.7	18.3	11.9
Hf	4	5.6	4.8	4.4	4.7	4.7	4.1	4.6	4.1	5.1	2.5
Zr	159.1	208.6	189.5	164	179.9	170.3	139.5	170.6	156.8	186.1	94
Y	19	23	20.3	17.3	18.1	18.9	26.1	15.8	19.1	14.7	14
Th	6.2	5.9	5.2	3.4	4.9	5.5	5	4.9	4.5	4.3	2.5
U	1.3	1.4	1.3	1.2	1.6	1	1.1	1.1	1.6	1.1	1.2
La	25.9	33.9	33.2	28.8	29.3	26.3	33.7	31.3	28.3	25.2	17.6
Ce	47.6	64.5	56.4	48.4	49.7	48.4	48.6	52.1	49.5	44.3	33.6
Pr	5.59	7.73	6.72	5.88	5.77	5.73	6.92	5.85	6.2	5.33	4.28
Nd	21.7	28.8	27	23.2	22.5	21.3	28.1	21.1	25.3	21	18
Sm	3.8	6.7	5.5	4.7	3.6	4.3	6.4	3.6	4.7	3.7	3.9
Eu	1.22	1.6	1.41	1.34	1.47	1.14	1.74	1.01	1.52	1.31	1.03
Gd	3.54	4.6	3.91	3.68	3.87	3.43	5.4	2.98	4.15	3.51	3.23
Tb	0.59	0.78	0.61	0.5	0.55	0.58	0.75	0.51	0.59	0.51	0.45
Dy	3.65	3.86	3.47	3.33	2.96	3.32	4.26	2.71	3.5	2.54	2.55
Ho	0.77	0.76	0.66	0.58	0.62	0.64	0.91	0.56	0.7	0.5	0.48
Er	1.94	2.13	2.12	1.63	1.84	2.11	2.57	1.63	1.8	1.42	1.35
Tm	0.28	0.29	0.29	0.2	0.27	0.28	0.34	0.22	0.24	0.21	0.22
Yb	1.91	1.92	2.02	1.54	1.81	2.07	2.34	1.31	1.89	1.55	1.35
Lu	0.31	0.28	0.33	0.28	0.29	0.23	0.37	0.22	0.26	0.23	0.19

* Boquerón (BQN) & Río Loco (RL) data adapted from Jolly et al. (2007).

TABLE X | **Continued**

Sample*	RL01-02	RL5A	RL06-02	RL366/1.3	RL365/7.1	RL03-02	RL43-94	Rl365/3.6	RL366/1.4	RL365/3.8	RL366/1.3
SiO_2	53.68	53.71	54.32	55.03	55.08	55.61	56.47	56.67	57.01	57.04	57.41
TiO_2	0.61	0.61	0.78	0.62	0.80	0.61	0.81	0.75	0.77	0.72	0.69
Al_2O_3	10.93	10.75	12.08	11.17	11.76	10.86	11.62	11.85	12.93	11.72	11.78
Fe_2O_3	9.11	7.10	9.62	8.89	9.74	9.16	8.61	8.61	8.03	8.60	8.34
MnO	0.14	0.12	0.15	0.14	0.14	0.14	0.13	0.13	0.12	0.12	0.14
MgO	10.33	7.52	8.34	9.12	7.79	9.59	7.47	7.85	6.97	7.84	6.97
CaO	7.50	9.11	6.93	7.31	7.53	7.46	7.46	6.83	5.93	6.79	7.64
Na_2O	2.35	3.00	2.19	2.45	2.19	2.35	1.90	1.86	2.41	1.67	3.04
K_2O	0.52	0.67	1.97	1.24	1.48	0.65	2.02	2.00	3.12	2.00	0.72
P_2O_5	0.29	0.28	0.29	0.26	0.26	0.29	0.24	0.28	0.31	0.28	0.27
LOI	4.1	6.9	2.8	3.5	3.0	2.8	3.2	2.9	2.1	2.9	2.6
Total	99.56	99.77	99.47	99.73	99.77	99.52	99.93	99.73	99.70	99.68	99.60
Cr	246	246	280	510	420	270	287	363	253	368	335
Ni	158	38	120	63	46	174	100	45	51	49	40
Co	40	27	39	37	41	41	33	32	30	33	30
Sc	30	20	27	27	30	31	26	27	21	26	24
V	195	184	223	189	234	185	174	212	208	201	205
Cu	0	72	0	57	77	0	85	67	88	70	58
Pb	3	22	2	94	4	4	2	5	15	9	157
Zn	0	41	0	48	54	0	70	52	54	55	43
Rb	12	13	43	24	24	12	40	53	54	48	13
Cs	0	0	0.9	0.2	0.2	0	0.2	0.8	0.5	0.7	0.1
Ba	662	904	1434	825	762	747	1222	1886	1452	1803	876
Sr	521	540	455	450	472	549	421	682	615	707	591
Ga	15	13	16	16	17	13	14	16	17	17	14
Ta	0.7	1.1	0.7	0.8	0.7	0.7	0.9	1.2	1	1	0.8
Nb	12.5	14	11.9	11.6	10.8	12.2	13.6	17.2	16.1	15.7	13.1
Hf	2.7	3.3	2.4	2.3	2.5	2.2	2.7	3.5	2.9	3.4	2.8
Zr	95	111	92	95	91	95	100	131	122	124	111
Y	12	14	13	12	15	12	12	15	17	15	13
Th	4	4.6	3.6	3.6	3.4	3.1	3.3	5.1	4.4	4.5	4.7
U	1.6	1.7	0.9	0.8	0.8	1.2	1.4	1	1.3	1.3	1.7
La	22.4	23.4	18.5	22.2	18.3	22	20.6	26.4	24.4	26.6	23.1
Ce	38.5	41.8	32.7	39.4	32.3	38	35.7	48.2	42.6	45.2	41.4
Pr	4.59	5.16	4.12	4.77	4.17	4.57	4.5	5.73	4.94	5.5	5.2
Nd	19.1	20.3	17.2	19.1	16.5	18.8	18.7	21.8	29.6	21.5	19.7
Sm	3.6	4.3	3.6	3.5	3.4	3.8	3.3	4.5	3.5	4.1	4.1
Eu	0.99	1.04	0.98	0.97	1.02	0.93	0.93	0.81	0.88	0.84	1.12
Gd	2.94	3	3.26	3.15	3.19	2.66	2.67	3.85	3.51	3.54	3.12
Tb	0.39	0.39	0.44	0.4	0.44	0.38	0.36	0.46	0.47	0.43	0.38
Dy	1.78	2.52	2.25	2.1	2.41	2	1.97	2.37	2.53	2.52	2.46
Ho	0.4	0.39	0.43	0.36	0.53	0.4	0.37	0.49	0.51	0.48	0.44
Er	0.98	1.2	1.19	1.15	1.45	1.09	1.07	1.39	1.32	1.22	1.29
Tm	0.14	0.2	0.15	0.19	0.19	0.17	0.14	0.21	0.2	0.19	0.17
Yb	0.98	1.21	1.06	1.24	1.56	0.98	1.04	1.29	1.36	1.19	1.11
Lu	0.17	0.15	0.18	0.15	0.21	0.17	0.16	0.21	0.19	0.17	0.18

* Boquerón (BQN) & Río Loco (RL) data adapted from Jolly et al. (2007).

DOI: 10.1344/105.000001715

TABLE X | **Continued**

Sample*	RL366/2.5	RL366/2.0	RL365/3.2	RL365/3.2	RL79-94	RL366/5.4
SiO_2	57.43	57.52	58.05	58.05	58.37	58.50
TiO_2	0.69	0.74	0.73	0.73	0.87	0.77
Al_2O_3	11.69	12.05	12.15	12.15	11.97	11.79
Fe_2O_3	8.02	8.54	8.02	8.02	8.31	8.34
MnO	0.12	0.12	0.12	0.12	0.13	0.12
MgO	7.85	7.18	6.63	6.63	6.82	6.38
CaO	7.66	7.26	6.62	6.62	6.90	5.30
Na_2O	1.72	2.43	3.27	3.27	1.75	2.80
K_2O	1.81	1.25	1.11	1.11	2.15	2.72
P_2O_5	0.27	0.28	0.28	0.28	0.28	0.29
LOI	2.4	2.4	2.8	2.8	2.0	2.2
Total	99.66	99.77	99.78	99.78	99.55	99.21
Cr	335	335	253	288	275	300
Ni	48	41	40	40	112	51
Co	30	31	29	29	30	32
Sc	25	25	24	24	26	24
V	196	202	189	189	204	225
Cu	75	52	68	68	0	82
Pb	3	3	11	11	4	4
Zn	47	49	51	51	0	51
Rb	39	28	21	21	53	69
Cs	0.1	0.2	0.3	0.3	1	0.7
Ba	1791	981	771	771	1191	1440
Sr	662	621	465	465	589	389
Ga	16	18	16	16	15	18
Ta	0.9	1.1	1	1	1.2	1.1
Nb	15	16	15.9	15.9	17.1	16.5
Hf	3.3	3.5	2.9	2.9	3.2	3.3
Zr	122	125	122	122	129	132
Y	15	15	15	15	14	14
Th	5.5	4.4	4.1	4.1	4.3	3.5
U	1	1.1	1.7	1.7	2.4	1.7
La	24.6	25.1	24.6	24.6	25.5	27
Ce	42.8	44.8	45.8	45.8	46.9	49
Pr	5.17	5.16	5.18	5.18	5.62	5.77
Nd	21.7	20.6	20.2	20.2	24.3	22
Sm	4.3	4.9	3.7	3.7	4.1	4.3
Eu	0.86	1.05	1.16	1.16	1.13	1.05
Gd	3.35	3.15	3.27	3.27	3.05	3.18
Tb	0.38	0.44	0.48	0.48	0.48	0.47
Dy	2.11	2.34	2.86	2.86	2.53	2.63
Ho	0.42	0.47	0.47	0.47	0.46	0.47
Er	1.2	1.16	1.52	1.52	1.29	1.38
Tm	0.19	0.2	0.23	0.23	0.18	0.18
Yb	1.17	1.28	1.15	1.15	1.08	1.19
Lu	0.17	0.16	0.15	0.15	0.2	0.19

* Boquerón (BQN) & Río Loco (RL) data adapted from Jolly et al. (2007).